NASA TECHNICAL NOTE

NASA TN D-3893

NASA TN D-3893

A NUMERICAL METHOD FOR DETERMINING THE AEROELASTIC DIVERGENCE CHARACTERISTICS OF UNGUIDED, SLENDER-BODY, MULTISTAGE LAUNCH VEHICLES

by Clarence P. Young, Jr.

Langley Research Center
Langley Station, Hampton, Va.

NATIONAL AERONAUTICS AND SPACE ADMINISTRATION • WASHINGTON, D. C. • APRIL 1967

NASA TN D-3893

A NUMERICAL METHOD FOR DETERMINING THE AEROELASTIC DIVERGENCE CHARACTERISTICS OF UNGUIDED, SLENDER-BODY, MULTISTAGE LAUNCH VEHICLES

By Clarence P. Young, Jr.

Langley Research Center
Langley Station, Hampton, Va.

NATIONAL AERONAUTICS AND SPACE ADMINISTRATION

For sale by the Clearinghouse for Federal Scientific and Technical Information
Springfield, Virginia 22151 – CFSTI price $3.00

A NUMERICAL METHOD FOR DETERMINING THE AEROELASTIC DIVERGENCE CHARACTERISTICS OF UNGUIDED, SLENDER-BODY, MULTISTAGE LAUNCH VEHICLES*

By Clarence P. Young, Jr.
Langley Research Center

SUMMARY

A theoretical method for analyzing the aeroelastic divergence behavior of unguided, slender-body, multistage launch vehicles is presented. A rigorous matrix recurrence solution to the system equations based on a finite-difference approach yields the stability boundary at which aeroelastic divergence would occur. The stability criterion for acceptable design is reviewed and results of comparative analytical studies are illustrated. Secondary influences on aeroelastic divergence, such as thrust and aerodynamic cross-flow, are incorporated and results of studies to ascertain the significance of these secondary influences are included. Example input data are presented and discussed along with illustrated output results. Comprehensive parameter studies are included to indicate corrective measures that may be used to avoid aeroelastic divergence.

INTRODUCTION

In recent years, aeroelastic studies have assumed an important role in the design of launch vehicles. Although considerable work has been done in the investigation of the flight dynamics and flutter phenomenon of aircraft, there has been a noticeable lag in the development of rigorous analytical methods for investigating the divergence problems associated with the flight of unguided, slender-body, multistage launch vehicles. Since most launch vehicles are designed to perform orbital, probe, and reentry missions, the dynamic conditions imposed on the vehicle are normally very stringent and require a high degree of sophistication in the aeroelastic divergence analysis.

---

*A major portion of the information presented herein was included in a thesis entitled "The Development of an Analytical Method for Determining the Aeroelastic Divergence Characteristics of Unguided, Slender Body, Multistage Flight Vehicles," offered in partial fulfillment of the requirements for the degree of Master of Science in Engineering Mechanics, Virginia Polytechnic Institute, Blacksburg, Virginia, June 1964.

A knowledge of the aeroelastic divergence characteristics of flight vehicles is essential to their design, since divergence is a function of the structural stiffness, mass distribution, distributed aerodynamic characteristics, and engine thrust. Also, it is important to realize that conventional structural-design considerations are influenced primarily by the strength of the structure, whereas aeroelastic design focuses on the rigidity, aerodynamic shape, dynamic behavior, and damping characteristics of the structure. Failure to consider aeroelastic effects could very well lead to the destruction of the vehicle.

The analytical method developed herein deals with the nonoscillatory stability problem arising from the interaction of aerodynamic forces and axial loading with the elastic deformation of the structure, classically known as steady-state or static aeroelastic instability.

A limited number of related theoretical studies are available on the aeroelastic divergence of slender-body, multistage launch vehicles. In the research report by Arbic, White, and Gillespie (ref. 1), investigations were made to determine approximate methods of estimating the effects of aeroelastic bending of small rocket-propelled model-booster configurations. Limited theoretical and experimental correlations were obtained for flights of several model-booster configurations. Thomson (ref. 2) developed an approximate slender-body divergence theory, although it requires numerous geometric and analytical assumptions. The theory of reference 2 appears to give conservative results (that is, early divergence is predicted) when correlated with a limited number of actual flight failures, which Thomson attributes to the possible poor estimates of aerodynamic normal-force derivatives, an oversimplified theory, or a combination of both.

Alley and Gerringer (ref. 3) have developed a rigorous approach to the problem of vehicle flight divergence. The matrix method of reference 3 employs a discrete-element representation of the structural system and is designed around the use of influence coefficients to represent vehicle flexibility. Also, the authors correlate the divergence dynamic pressure with the generalized static margin for the elastic structure and set forth stability criteria appropriate for both rigid- and flexible-body analyses.

Keith et al. (ref. 4) develop the equations governing the aeroelastic behavior of launch vehicles from Lagrange's principles in terms of generalized coordinates. As noted in reference 4, the collocation method of analysis discussed by Keith is principally due to Alley and Gerringer's method of reference 3. Also, Keith employs the modal method of analysis which is characterized by the use of the vibration modes of the unforced system as a representation of vehicle flexibility.

Another technique for computing aeroelastic divergence and stability characteristics of nonuniform beamlike structures is presented herein. This method is inherently appropriate to structures that exhibit numerous discontinuities in the mass, aerodynamic,

and stiffness distributions. A main advantage is that the technique requires no conversion to an analogous lumped or discrete panel system such as that required by the methods of references 3 and 4. A matrix recurrence formula obtained from a finite-difference approach is used to effect the numerical solution of the differential equations of the system. Also, the presentation of the problem in matrix form has proved highly adaptable for high-speed digital computers. Furthermore, the formulation includes the secondary influences of thrust and aerodynamic crossflow which have not been treated in other investigations, with the exception of reference 4.

The mathematical derivations are presented along with information pertinent to the practical numerical solution obtained by means of a digital computer. Results of comparative analyses and data for assessing the significance of secondary influences are included. An example application of the method to a typical four-stage launch vehicle is submitted along with the results of parameter studies that illustrate effective means of improving divergent designs. An appendix is included to illustrate the superposition of boundary conditions applied to this method of solution.

SYMBOLS

The units of measurement originally used in the development were in the U.S. Customary System. However, alternate values are provided in the International System (SI) to increase the usefulness of the paper. Details of the SI system and necessary conversion factors are available in reference 5.

$\left.\begin{matrix} a,b,c,d, \\ e,g,k \end{matrix}\right\}$ matrix elements defined by equation (28)

$\left(C_{L_\alpha} S\right)_1$ product of first-stage-fin lift-force-coefficient slope and first-stage-fin reference area, in^2/rad (m^2/rad)

$\left(C_{L_\alpha} S\right)_{1,d}$ product of first-stage-fin lift-force-coefficient slope and first-stage-fin reference area for nominal design, in^2/rad (m^2/rad)

$\left(C_{L_\alpha} S\right)_2$ product of second-stage-fin lift-force-coefficient slope and second-stage-fin reference area, in^2/rad (m^2/rad)

$\left(C_{L_\alpha} S\right)_f$ product of flare lift-force-coefficient slope and flare reference area, in^2/rad (m^2/rad)

$(C_{L_\alpha} S)_{f,d}$ product of flare lift-force-coefficient slope and flare reference area for nominal design, in^2/rad (m^2/rad)

D local body diameter, in. (m); also used for the determinant defined in equation (29)

D_{max} maximum body diameter, in. (m)

E modulus of elasticity in bending, lbf/in^2 (N/m^2)

EI flexural stiffness coefficient, $lbf\text{-}in^2$ $(N\text{-}m^2)$

$(EI)_d$ nominal design stiffness coefficient, $lbf\text{-}in^2$ $(N\text{-}m^2)$

$(EI)_e$ equivalent flexural stiffness coefficient defined by equation (39), $lbf\text{-}in^2$ $(N\text{-}m^2)$

h aerodynamic moment-coefficient reference length, in. (m)

I moment of inertia of a given cross-sectional area, in^4 (m^4)

K matrix in equation (26a)

L total length of vehicle, in. (m)

M bending moment, in-lbf (m-N)

m distributed mass, $lbf\text{-}sec^2/in^2$ $(N\text{-}sec^2/m^2)$

m_t total mass defined by equation (5a), $lbf\text{-}sec^2/in.$ $(N\text{-}sec^2/m)$

o a point on the structural element identified in the derivation

P axial load exclusive of internal and external static pressures, lbf (N)

q flight dynamic pressure, $\frac{1}{2}\rho u^2$, lbf/in^2 (N/m^2)

q_{div} dynamic pressure of divergence, lbf/in^2 (N/m^2)

$q_{div,o}$ dynamic pressure of divergence with secondary effects excluded, lbf/in^2 (N/m^2)

R	radius of curvature of flight path at $x = x_a$, in. (m)
$1/R$	curvature of the flight path at $x = x_a$, in^{-1} (m^{-1})
S	characteristic reference area, in^2 (m^2)
$(SC_D)_b$	product of associated base reference area and base drag-force coefficient, in^2 (m^2)
$(SC_D)_t$	product of associated reference area and total nonviscous drag-force coefficient (see eq. (5b)), in^2 (m^2)
$S\frac{dC_D}{dx}$	product of associated reference area and distributed forebody drag-force-coefficient slope, in. (m)
$S\frac{dC_{L_\alpha}}{dx}$	product of associated reference area and distributed lift-force-coefficient slope, in./rad (m/rad)
$Sh\frac{d\overset{*}{C}_{M_\alpha}}{dx}$	product of local reference area, reference length, and local moment coefficient arising from axial components of aerodynamic pressures acting on an inclined surface of revolution at an angle of attack α, defined by equation (3), in^2 (m^2)
T	thrust, lbf (N)
t	flight time, sec
u	velocity of the vehicle tangent to the flight path at $x = x_a$, in./sec (m/sec)
V	shear force, lbf (N)
X	column matrix of variables (see eqs. (16) and (17))
X,Y	system axes
x	independent coordinate along the length of the vehicle, taken tangent to the flight path at $x = x_a$ (see figs. 1 and 3), in. (m)
x_{cg}	coordinate to center of gravity, in. (m)

x_{cp} coordinate to center of pressure, in. (m)

$x_{sm,rig}$ rigid-vehicle static margin, $x_{cg} - x_{cp}$, in. (m)

y elastic deformation of vehicle measured relative to X-axis, in. (m)

α local angle of attack defined by equation (6), rad

β rectangular matrix (see eqs. (16) and (17))

$\dot{\gamma}$ angular velocity about an axis normal to X,Y axes, rad/sec

δ_1 rectangular matrix defined by equation (22b)

δ_2 rectangular matrix defined by equation (22d)

κ_u local rotational increment at $x = x_u$ due to joint flexibility, rad/in-lbf (rad/m-N)

Λ_n column matrix (see eq. (22e))

$\lambda_n( )$ approximation of second derivative of variable ( ) at station n with respect to x (see eqs. (18) to (21a) and (22e))

ρ air density, lbf-sec^2/in^4 (N-sec^2/m^4)

$\left| \ \right|$ determinant of a matrix

$\{ \}$ column matrix

$\lceil 1 \rfloor$ unit matrix

$[ ]$ square or rectangular matrix

$[ ]^{-1}$ inverse matrix

Subscripts:

A,B,C,D	separate solutions to equation (17) that are associated with the initial unit-boundary-value relationships set forth in the appendix
a	value of function at lower boundary
l	value of function at upper boundary
n	longitudinal station number, integer
ref	reference value
u	coordinate of uth joint
(+)	value of a discontinuous function on the positive side of a discontinuity
(-)	value of a discontinuous function on the negative side of a discontinuity

Primed symbols denote differentiation with respect to x.

Dotted symbols denote differentiation with respect to time.

ANALYSIS

The applicable assumptions and limitations of the analysis and the derivation of a system of first-order differential equations describing divergent behavior are presented in this section. In addition, a description of the integration technique employed in the finite-difference numerical solution is included. A recurrence formula is established in order to relate system variables at one station on the structure to those at an adjoining station. Boundary conditions for the free-free thrusting system are established and a stability equation is obtained for computing the divergence dynamic pressure of the system. Also, the mathematical relationships across points of discontinuity are established.

Assumptions and Limitations

The pertinent assumptions and limitations underlying the development of the governing equations are as follows:

Unguided vehicle.- No coupled-autopilot considerations have been included in the derivation. The solution is therefore restricted to unguided-vehicle systems.

Nonspinning vehicle.- The vehicle is considered to be nonspinning. The omission of gyroscopic effects and Magnus forces is therefore a principal assumption. However, it is believed that application to vehicles of low spin rates provides useful approximate results.

Planar motion.- The flight behavior of the vehicle is constrained to a single plane of motion along a curvilinear path. Only self-induced inplane loads that characterize the aeroelastic divergence stability problem are considered, and the effects of gravity are ignored.

Linear relationships.- The elastic deformations are considered to be small displacements in the neighborhood of an equilibrium condition. The elementary beam theory is therefore considered applicable in describing the elastic deformation of the structure.

Linear aerodynamic theory is assumed; that is, the local aerodynamic lift force is assumed to be proportional to the product of the local angle of attack and the appropriate aerodynamic lift-force derivative.

Shear deformation.- The contributions to deflection resulting from shear deformation are ignored in the derivations. It is believed that the omission of shear deformation will not significantly alter the results obtained by this method of analysis for typical vehicle geometries of high slenderness ratios.

Aerodynamic considerations.- "Quasi-static" aerodynamic loading functions are considered applicable. Aerodynamic coupling (downwash) due to aerodynamic changes arising from elastic deformations of the system is not considered in the formulation. Reductions in rearward-fin lift effectiveness due to downwash interference from forward fin arrangements can be approximately accounted for by utilizing appropriate effective fin-lift derivatives.

Steady-state analysis.- The mathematical formulation is based on the assumption that a nonoscillatory dynamic-equilibrium condition can characterize the system for a particular set of conditions associated with a given time in flight.

Inertia effects.- The centripetal acceleration at the origin of the reference coordinate system due to curvilinear flight is considered to act normal to the reference X-axis and to be constant over the vehicle length. The centripetal-acceleration components acting on an element due to its position relative to the rotating reference frame are considered insignificant. These considerations are consistent with the assumption of small elastic displacements, small angles of attack, and a vehicle length small in comparison with the flight-path radius. Thus, only the centrifugal inertia forces arising

from the angular velocity of the rotating reference frame and the axial inertial loadings induced by thrust and drag are considered necessary to maintain dynamic equilibrium.

Axial loading.- The contributing axial loads on the structure are taken as the inertia loads plus the drag due to nonviscous aerodynamic loading only. Structural bending that may arise from Bourdon tube pressure effects are considered trivial.

Misalinement and eccentricity effects.- Loads arising from thrust, fin, and body misalinements as well as mass eccentricities are nonhomogeneous contributions to the equilibrium equations. The static aeroelastic divergence behavior is represented by a system of homogeneous equations which precludes the effects of misalinement and eccentricity loading functions.

Derivation of Equations for a Free-Free Thrusting Vehicle System

The mathematical formulation that follows is restricted to the development of a homogeneous system of equations derived from equilibrium and geometric considerations that mathematically characterize static aeroelastic divergence behavior. Consideration of a nonhomogeneous system (that is, inclusion of external forces independent of the variables describing static aeroelastic divergence) would be of the nature of a response problem, which is beyond the scope of this paper.

The vehicle coordinate system and differential-element force diagram are presented in figure 1.

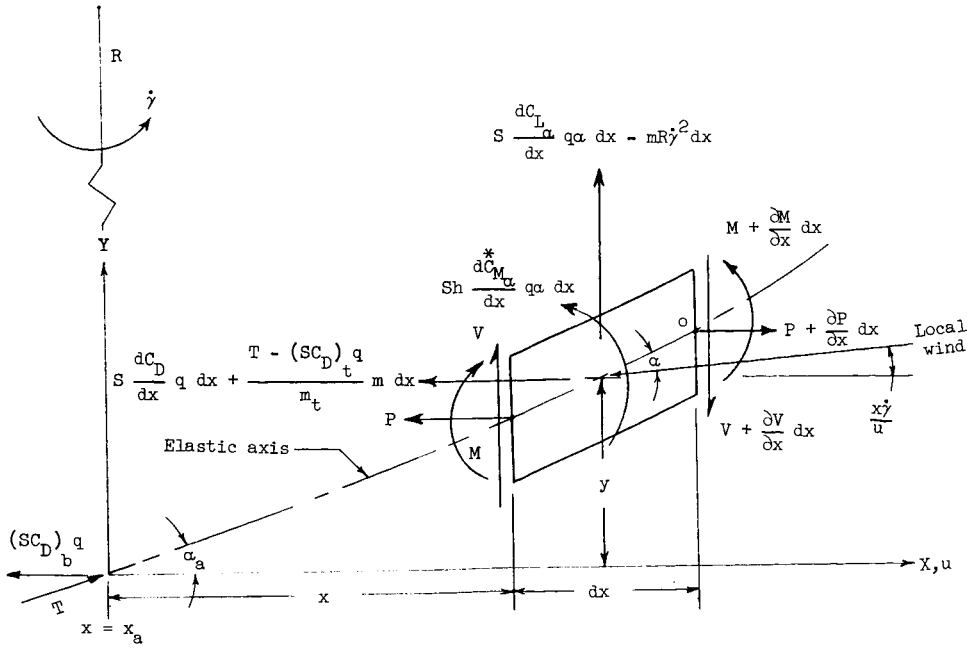

Figure 1.- Vehicle coordinate system and differential-element force diagram.

The motion is constrained to a curvilinear flight path that is established by the locus of the origin of the inplane velocity-oriented X,Y axes. The direction of the Y-axis is taken to coincide with that of the flight-path radius established at the origin, and the orthogonal X-axis is coincident with the direction of the velocity vector tangent to the flight path at the origin. The elastic vehicle is thus represented relative to a set of rotating velocity axes with the origin at or near the aft end of the vehicle.

Consider an element of the deformed structure of length dx subjected to local transverse aerodynamic lift and centrifugal forces and to aerodynamic drag and thrust-induced inertia forces as depicted in figure 1. By d'Alembert's principle, summing forces acting on the element normal to the X-axis yields

$$\frac{\partial V}{\partial x}\,dx + mR\dot{\gamma}^2 dx - S\,\frac{dC_{L_\alpha}}{dx}\,q\alpha\,dx = 0 \tag{1}$$

For pitching equilibrium, summing moments about a point o on the elastic axis and disregarding terms containing products of differentials (that is, $(dx)^2$) gives

$$V\,dx - Sh\,\frac{d\overset{*}{C}_{M_\alpha}}{dx}\,q\alpha\,dx - \frac{\partial M}{\partial x}\,dx + P\,\frac{\partial y}{\partial x}\,dx = 0 \tag{2}$$

In equation (2) the local aerodynamic moment coefficient $d\overset{*}{C}_{M_\alpha}/dx$ arises from the axial components of the aerodynamic pressures acting on an inclined surface of revolution at an angle of attack α. For small angles of attack, this component can be derived from the relationships given in the appendix of reference 6 and can be expressed in terms of the distributed aerodynamic lift-force-coefficient derivative as

$$Sh\,\frac{d\overset{*}{C}_{M_\alpha}}{dx} = \frac{D}{4}\,\frac{dD}{dx}\,S\,\frac{dC_{L_\alpha}}{dx} \tag{3}$$

Summing forces in the x-direction gives

$$\frac{\partial P}{\partial x}\,dx - \frac{T - (SC_D)_t\,q}{m_t}\,m\,dx - S\,\frac{dC_D}{dx}\,q\,dx = 0 \tag{4}$$

Since the axial force is a function of x and of the independent variable q, the evaluation of P at a point x may be written as

$$P(x) = \frac{T - (SC_D)_t\,q}{m_t}\int_{x_a}^{x} m\,dx + q\int_{x_a}^{x} S\,\frac{dC_D}{dx}\,dx + P_a \tag{5}$$

where T is the thrust, m_t is the total mass of the system defined by

$$m_t = \int_{x_a}^{x_l} m \, dx \tag{5a}$$

and $(SC_D)_t$ is the product of the associated reference area and the total nonviscous drag-force coefficient, defined as

$$(SC_D)_t = \int_{x_a}^{x_l} S \frac{dC_D}{dx} dx + (SC_D)_b \tag{5b}$$

The subscripts a and l denote values of the function at the lower and upper boundaries of the free-free system.

From figure 1, the local angle of attack on the element can be written as

$$\alpha = \frac{\partial y}{\partial x} - \frac{x\dot{\gamma}}{u} \tag{6}$$

where $\partial y/\partial x$ is the local slope of the elastic axis and $x\dot{\gamma}/u$ is the contribution to α at x due to the change in position of the local wind vector at a point on the vehicle that is restricted to move along a curvilinear flight path at an angular velocity $\dot{\gamma}$.

Differentiating equation (6) with respect to x gives

$$\frac{\partial \alpha}{\partial x} = \frac{\partial^2 y}{\partial x^2} - \frac{\dot{\gamma}}{u} \tag{7}$$

The relationship for the rate of change of the slope of the elastic axis is obtained from the elementary beam theory as

$$\frac{\partial^2 y}{\partial x^2} = \frac{M}{EI} \tag{8}$$

which when substituted into equation (7) yields

$$\frac{\partial \alpha}{\partial x} = \frac{M}{EI} - \frac{\dot{\gamma}}{u} \tag{9}$$

The curvature of the flight path is defined as

$$\frac{1}{R} = \frac{\dot{\gamma}}{u} \tag{10}$$

where $\dot{\gamma}$ is the angular velocity of the rotating reference frame and u is the velocity of the vehicle.

Differentiating equation (10) with respect to x gives the compatibility condition

$$\frac{\partial(1/R)}{\partial x} = 0 \tag{11}$$

Equation (11) expresses the invariance of the flight-path curvature over the length of the structure in accord with the imposed artificial flight-path constraint on the system.

By making the appropriate substitutions for $\dot{\gamma}$ (from eq. (10)) into equations (1) and (9) and for $\frac{\partial y}{\partial x}$ (from eq. (6)) into equation (2), the system equations become a function of V, α, M, and $1/R$. The partial derivatives may be replaced by their differentials since $1/R$ is invariant and V, α, and M vary only with x. The four governing differential equations then take the form

$$\frac{dV}{dx} + m\frac{u^2}{R} - S\frac{dC_{L_\alpha}}{dx}q\alpha = 0 \tag{12}$$

$$V - \frac{dM}{dx} + P\left(\alpha + \frac{x}{R}\right) - Sh\frac{d\overset{*}{C}_{M_\alpha}}{dx}q\alpha = 0 \tag{13}$$

$$\frac{d\alpha}{dx} - \frac{M}{EI} + \frac{1}{R} = 0 \tag{14}$$

$$\frac{d(1/R)}{dx} = 0 \tag{15}$$

Expressed in matrix notation, equations (12) to (15) appear as

$$\begin{bmatrix} 1 & 0 & 0 & -S\frac{dC_{L_\alpha}}{dx}q & 0 & 0 & 0 & mu^2 \\ 0 & 1 & 0 & P - Sh\frac{d\overset{*}{C}_{M_\alpha}}{dx}q & -1 & 0 & 0 & Px \\ 0 & 0 & 1 & 0 & 0 & \frac{-1}{EI} & 0 & 1 \\ 0 & 0 & 0 & 0 & 0 & 0 & 1 & 0 \end{bmatrix} \begin{Bmatrix} V' \\ V \\ \alpha' \\ \alpha \\ M' \\ M \\ (1/R)' \\ 1/R \end{Bmatrix} = \begin{Bmatrix} 0 \end{Bmatrix} \tag{16}$$

where the primes denote differentiation with respect to x. If the 4×8 matrix is denoted as β and the 8×1 matrix of unknowns is denoted as X, then equation (16) may be written as

$$[\beta]\{X\} = \{0\} \tag{17}$$

The matrix equation (17) represents the desired homogeneous set of equations that describe the aeroelastic divergence behavior of the free-free thrusting vehicle system along a curvilinear path. The solution of equation (17) leads to aeroelastic stability conclusions as formulated in subsequent sections.

Method of Integration and Development of the Recurrence Formula

The analysis presented herein employs a numerical method to solve equation (17). The integration technique was originally derived in reference 7.

Based on the assumption that the first derivatives of the system variables vary linearly over the small increment $\Delta x_n = x_{n+1} - x_n$, the following relationships can be written:

$$\frac{dV_{n+1}}{dx} = \frac{dV_n}{dx} + \Delta x_n \lambda_n(V) \tag{18}$$

Integrating over the interval Δx_n yields

$$V_{n+1} = V_n + \frac{dV_n}{dx}\Delta x_n + \frac{(\Delta x_n)^2}{2}\lambda_n(V) \tag{18a}$$

Similarly, for the other variables,

$$\frac{d\alpha_{n+1}}{dx} = \frac{d\alpha_n}{dx} + \Delta x_n \lambda_n(\alpha) \tag{19}$$

$$\alpha_{n+1} = \alpha_n + \frac{d\alpha_n}{dx}\Delta x_n + \frac{(\Delta x_n)^2}{2}\lambda_n(\alpha) \tag{19a}$$

$$\frac{dM_{n+1}}{dx} = \frac{dM_n}{dx} + \Delta x_n \lambda_n(M) \tag{20}$$

$$M_{n+1} = M_n + \frac{d(M_n)}{dx}\Delta x_n + \frac{(\Delta x_n)^2}{2}\lambda_n(M) \tag{20a}$$

$$\frac{d(1/R_{n+1})}{dx} = \frac{d(1/R_n)}{dx} + \Delta x_n \lambda_n(1/R) \tag{21}$$

$$\frac{1}{R_{n+1}} = \frac{1}{R_n} + \frac{d(1/R_n)}{dx}\Delta x_n + \frac{(\Delta x_n)^2}{2}\lambda_n(1/R) \tag{21a}$$

The functions $\lambda_n(V)$, $\lambda_n(\alpha)$, $\lambda_n(M)$, and $\lambda_n(1/R)$ are as yet undetermined but they will be uniquely established herein.

Equations (18) to (21a) may be written in matrix notation as

$$\left\{X_{n+1}\right\} = \left[\delta_1\right]\left\{X_n\right\} + \Delta x_n\left[\delta_2\right]\left\{\Lambda_n\right\} \tag{22}$$

where

$$\left\{X_{n+1}\right\} = \begin{Bmatrix} V'_{n+1} \\ V_{n+1} \\ \alpha'_{n+1} \\ \alpha_{n+1} \\ M'_{n+1} \\ M_{n+1} \\ \left(1/R_{n+1}\right)' \\ 1/R_{n+1} \end{Bmatrix} \tag{22a}$$

$$\left[\delta_1\right] = \begin{bmatrix} 1 & 0 & 0 & 0 & 0 & 0 & 0 & 0 \\ \Delta x_n & 1 & 0 & 0 & 0 & 0 & 0 & 0 \\ 0 & 0 & 1 & 0 & 0 & 0 & 0 & 0 \\ 0 & 0 & \Delta x_n & 1 & 0 & 0 & 0 & 0 \\ 0 & 0 & 0 & 0 & 1 & 0 & 0 & 0 \\ 0 & 0 & 0 & 0 & \Delta x_n & 1 & 0 & 0 \\ 0 & 0 & 0 & 0 & 0 & 0 & 1 & 0 \\ 0 & 0 & 0 & 0 & 0 & 0 & \Delta x_n & 1 \end{bmatrix} \tag{22b}$$

$$\left\{X_n\right\} = \begin{Bmatrix} V'_n \\ V_n \\ \alpha'_n \\ \alpha_n \\ M'_n \\ M_n \\ \left(1/R_n\right)' \\ 1/R_n \end{Bmatrix} \tag{22c}$$

$$\left[\delta_2\right] = \begin{bmatrix} 1 & 0 & 0 & 0 \\ \frac{\Delta x_n}{2} & 0 & 0 & 0 \\ 0 & 1 & 0 & 0 \\ 0 & \frac{\Delta x_n}{2} & 0 & 0 \\ 0 & 0 & 1 & 0 \\ 0 & 0 & \frac{\Delta x_n}{2} & 0 \\ 0 & 0 & 0 & 1 \\ 0 & 0 & 0 & \frac{\Delta x_n}{2} \end{bmatrix} \tag{22d}$$

$$\left\{\Lambda_n\right\} = \begin{Bmatrix} \lambda_n(V) \\ \lambda_n(\alpha) \\ \lambda_n(M) \\ \lambda_n(1/R) \end{Bmatrix} \tag{22e}$$

The system variables must satisfy the geometric and equilibrium equations at any specified station; that is, when $x = x_{n+1}$ from equation (17),

$$\left[\beta_{n+1}\right]\left\{X_{n+1}\right\} = \left\{0\right\} \tag{23}$$

by virtue of the constraint imposed through the following determination of the Λ_n matrix. Substituting equation (22) into equation (23) and solving for Λ_n yields

$$\left\{\Lambda_n\right\} = \frac{-1}{\Delta x_n}\left[\left[\beta_{n+1}\right]\left[\delta_2\right]\right]^{-1}\left[\beta_{n+1}\right]\left[\delta_1\right]\left\{X_n\right\} \tag{24}$$

Thus, the variables $\lambda_n(V)$, $\lambda_n(\alpha)$, $\lambda_n(M)$, and $\lambda_n(1/R)$, which were previously undetermined, are now defined by virtue of the required satisfaction of equation (23).

Substituting equation (24) into equation (22) gives the recurrence formula for the functions V, α, M, and 1/R.

$$\left\{X_{n+1}\right\} = \left[\left[1\right] - \left[\delta_2\right]\left[\left[\beta_{n+1}\right]\left[\delta_2\right]\right]^{-1}\left[\beta_{n+1}\right]\right]\left[\delta_1\right]\left\{X_n\right\} \tag{25}$$

Equation (25) can be written in abbreviated matrix form as

$$\left\{X_{n+1}\right\} = \left[K_{n+1}\right]\left\{X_n\right\} \tag{26}$$

where

$$\left[K_{n+1}\right] = \left[\left[1\right] - \left[\delta_2\right]\left[\left[\beta_{n+1}\right]\left[\delta_2\right]\right]^{-1}\left[\beta_{n+1}\right]\right]\left[\delta_1\right] \tag{26a}$$

Equation (26) is the recurrence relationship that will lead to the solution of equation (17) with the appropriate treatment of the initial and terminal boundary conditions. The elements contained in the K_{n+1} matrix are functions of the aerodynamic and inertial loading and the elastic stiffness characteristics of the system for the appropriate $n+1$ value of the x-coordinate. The useful working relationships for the K_{n+1} matrix obtained through required matrix manipulations are developed as follows:

From equations (16), (17), and (22d) it can be shown that

$$\left[\beta_{n+1}\right]\left[\delta_2\right] = \begin{bmatrix} 1 & ad & 0 & de \\ d & d(b+g) & -1 & bdk \\ 0 & 1 & cd & d \\ 0 & 0 & 0 & 1 \end{bmatrix} \tag{27}$$

where

$$\left.\begin{aligned} a &= -\left(S\frac{dC_{L_\alpha}}{dx}\right)_{n+1} q \\ b &= P_{n+1} \\ c &= -(EI)^{-1}_{n+1} \\ d &= \frac{\Delta x_n}{2} \\ e &= m_{n+1}u^2 \\ g &= \left(-Sh\frac{d\overset{*}{C}_{M_\alpha}}{dx}\right)_{n+1} q \\ k &= x_{n+1} \end{aligned}\right\} \tag{28}$$

The determinant D of the matrix on the right-hand side of equation (27) is given in the expanded form by

$$D = cd^2(b + g - ad) + 1 \tag{29}$$

By utilizing equations (16), (17), (22b), (22d), (27), and (28) and performing the indicated matrix operations of equation (26a), the elements of the matrix K_{n+1} can be reduced to the explicit algebraic form of equation (30). The matrix of equation (30) can be evaluated by substitution of the appropriate values of the functions defined by equation (28). Equations (29) and (30) provide the working relationships for practical use of the recurrence formula given by equation (26).

$$\left[K_{n+1}\right] = \frac{1}{D}\begin{bmatrix} acd^3 & acd^2 & -ad & -a & acd^2 & acd & d[ad+acd^2bk-cd^2e(b+g)-e] & d[a+acdbk-cde(b+g)]-e \\ d[cd^2(b+g)+1] & cd^2(b+g)+1 & -ad^2 & -ad & acd^3 & acd^2 & d^2[ad+acd^2bk-cd^2e(b+g)-e] & d[ad+acd^2bk-cd^2e(b+g)-e] \\ -cd^2 & -cd & cd^2[ad-(b+g)] & cd[ad-(b+g)] & -cd & -c & d(cd^2e-cdbk-1) & d(cde-bck)-1 \\ -cd^3 & -cd^2 & d & 1 & -cd^2 & -cd & d^2(cd^2e-cdbk-1) & d(cd^2e-bcdk-1) \\ d & 1 & d(b+g-ad) & b+g-ad & cd^2[ad-(b+g)] & cd[ad-(b+g)] & d[ad^2+bk-d(b+g)-de] & -d(b+g-ad+e)+bk \\ d^2 & d & d^2(b+g-ad) & d(b+g-ad) & d & 1 & d^2[ad^2+bk-d(b+g)-de] & -d^2(b+g-ad+e)+bkd \\ 0 & 0 & 0 & 0 & 0 & 0 & 0 & 0 \\ 0 & 0 & 0 & 0 & 0 & 0 & d[cd^2(b+g)-acd^3+1] & D \end{bmatrix} \tag{30}$$

Boundary Conditions

The boundary conditions for the free-free thrusting vehicle system may be determined from the system equations and physical considerations at the end points. The subscripts a and l indicate that the associated quantity is evaluated at the lower boundary $x = x_a$ or at the upper boundary $x = x_l$.

Observe from figure 1 that at the lower boundary,

$$\text{Condition (a):} \quad V_a = T\alpha_a$$

Also at the upper boundary, for the free-free system,

$$\text{Condition (b):} \quad V_l = 0$$

The boundary conditions at both ends of the free-free system require that

$$\text{Condition (c):} \quad M_a = M_l = 0$$

From equation (15), it follows that

$$\text{Condition (d):} \quad \left(\frac{1}{R_a}\right)' = \left(\frac{1}{R_l}\right)' = 0$$

It follows from condition (d) that

$$\text{Condition (e):} \quad \frac{1}{R_a} = \frac{1}{R_l} = \frac{1}{R}$$

Observe from figure 1 that

$$\text{Condition (f):} \quad P_a = -T + \left(SC_D\right)_b q$$

Substituting condition (f) into equation (5) and evaluating over the total length of the vehicle gives

$$\text{Condition (g):} \quad P_l = 0$$

The angle of attack at the boundaries may be expressed as

$$\text{Condition (h):} \quad \alpha = \alpha_a$$

$$\text{Condition (i):} \quad \alpha = \alpha_l$$

Substituting the appropriate boundary relationship given by condition (e) into equation (12) yields

$$\text{Condition (j):} \quad V_a' = \left(S \frac{dC_{L_\alpha}}{dx}\right)_a q\alpha_a - m_a \frac{u^2}{R}$$

$$\text{Condition (k):} \quad V_l' = \left(S \frac{dC_{L_\alpha}}{dx}\right)_l q\alpha_l - m_l \frac{u^2}{R}$$

Substituting conditions (c) and (e) into equation (14) gives

$$\text{Condition } (l): \quad \alpha_a' = \alpha_l' = -\frac{1}{R}$$

Substituting conditions (a), (e), and (f) into equation (13) yields

$$\text{Condition (m):} \quad M_a' = \frac{-Tx_a}{R} + \left(SC_D\right)_b q\left(\alpha_a + \frac{x_a}{R}\right) - \left(Sh \frac{d\overset{*}{C}_{M_\alpha}}{dx}\right)_a q\alpha_a$$

Substituting conditions (b) and (g) into equation (13) gives

$$\text{Condition (n):} \quad M_l' = -\left(Sh \frac{d\overset{*}{C}_{M_\alpha}}{dx}\right)_l q\alpha_l$$

The boundary relationships for the system variables may now be summarized in matrix form. For the lower boundary conditions at $x = x_a$, it follows that

$$\begin{Bmatrix} V_a' \\ V_a \\ \alpha_a' \\ \alpha_a \\ M_a' \\ M_a \\ (1/R_a)' \\ 1/R_a \end{Bmatrix} = \begin{bmatrix} \left(S\frac{dC_{L_\alpha}}{dx}\right)_a q & -m_a u^2 \\ T & 0 \\ 0 & -1 \\ 1 & 0 \\ \left[(SC_D)_b - \left(Sh\frac{d\overset{*}{C}_{M_\alpha}}{dx}\right)_a\right] q & \left[(SC_D)_b q - T\right] x_a \\ 0 & 0 \\ 0 & 0 \\ 0 & 1 \end{bmatrix} \begin{Bmatrix} \alpha_a \\ 1/R \end{Bmatrix} \tag{31}$$

and for the conditions at $x = x_l$,

$$\begin{Bmatrix} V_l' \\ V_l \\ \alpha_l' \\ \alpha_l \\ M_l' \\ M_l \\ (1/R_l)' \\ 1/R_l \end{Bmatrix} = \begin{bmatrix} \left(S\frac{dC_{L_\alpha}}{dx}\right)_l q & -m_l u^2 \\ 0 & 0 \\ 0 & -1 \\ 1 & 0 \\ -\left(Sh\frac{d\overset{*}{C}_{M_\alpha}}{dx}\right)_l q & 0 \\ 0 & 0 \\ 0 & 0 \\ 0 & 1 \end{bmatrix} \begin{Bmatrix} \alpha_l \\ 1/R \end{Bmatrix} \tag{32}$$

Equations (31) and (32) represent the lower and upper boundary conditions that are essential to the complete solution of equation (17).

Development of the Stability Equation for a Free-Free Thrusting Vehicle System

The method of determining the stability equation is based upon superposition of the solutions of equation (26) for individual boundary values. A solution of the recurrence formula of equation (26) for the X variables at some station s in terms of either known

or assumed values of X at some station c is simply the repeated premultiplication of X_c:

$$\left\{X_s\right\} = \left[\left[K_s\right]\left[K_{s-1}\right] \cdots \left[K_{c+2}\right]\left[K_{c+1}\right]\right]\left\{X_c\right\} \tag{33}$$

Such a solution is strictly dependent upon the vector X_c, the system constants, and the dynamic pressure q contained in the K matrix. Consider two separate solutions of the form of equation (33) for an assumed q and over the length of the vehicle such that $X_c = X_a$ and $X_s = X_l$. Let the first solution be called the A solution for the single unit boundary relationship where $\alpha_a = 1$ when $1/R = 0$. Let the second solution be called the B solution for the single unit boundary relationship where $\alpha_a = 0$ when $1/R = 1$. Then because of the validity of superposition of solutions for independent boundary conditions, proof of which is given in the appendix, the value of $\{X\}$ at $x = x_n$ can be stated in terms of the A and B solutions on the actual lower boundary values, α_a and $1/R$, as

$$\left\{X_n\right\} = \alpha_a\left\{X_n\right\}_A + \frac{1}{R}\left\{X_n\right\}_B \tag{34}$$

With the use of the upper boundary conditions (b) and (c) of the preceding section, the following conditions can be related at $x = x_l$:

$$\begin{bmatrix} 0 & 1 & 0 & 0 & 0 & 0 & 0 & 0 \\ 0 & 0 & 0 & 0 & 0 & 1 & 0 & 0 \end{bmatrix}\left\{X_l\right\} = \begin{Bmatrix} V_l \\ M_l \end{Bmatrix} = \left\{0\right\} \tag{35}$$

Substituting equation (34) into equation (35) for the value of n at $x = x_l$ gives

$$\begin{Bmatrix} V_l \\ M_l \end{Bmatrix} = \begin{bmatrix} V_{l,A} & V_{l,B} \\ M_{l,A} & M_{l,B} \end{bmatrix}\begin{Bmatrix} \alpha_a \\ 1/R \end{Bmatrix} = \begin{bmatrix} A_1 & B_1 \\ A_2 & B_2 \end{bmatrix}\begin{Bmatrix} \alpha_a \\ 1/R \end{Bmatrix} = \left\{0\right\} \tag{36}$$

The subscripts A and B denote the values of V and M obtainable from the aforementioned unit solutions for α_a and $1/R$. The coefficients A_1 and A_2 are the values of V and M, respectively, at $x = x_l$ due to an assigned unit value of α at $x = x_a$. Similarly, B_1 and B_2 are the values of V and M, respectively, at $x = x_l$ due to a unit value of $1/R$ at $x = x_a$.

For finite values of α_a and $1/R$, the nontrivial solution of equation (36) is obtained by setting the determinant of the square matrix equal to zero:

$$\begin{vmatrix} A_1 & B_1 \\ A_2 & B_2 \end{vmatrix} = 0 \tag{37}$$

The elements in equation (37) are a function of the unknown dynamic pressure q, as is evident from inspection of the K_{n+1} matrix defined by equations (27), (28), and (29). The lowest nonzero characteristic value of q that satisfies equation (37) is the dynamic pressure of divergence q_{div} for the system. The physical significance of this mathematical finding is that performance of the vehicle at flight dynamic pressures greater than the divergence dynamic pressure is unstable.

For the relationships compatible with the divergence dynamic pressure, it is apparent from the homogeneous equation (36) that α_a and $1/R$ cannot be uniquely determined. However, the ratio of α_a to $1/R$ can be determined from equation (36). It is further evident that this equation is satisfied for values of α_a and $1/R$ having the appropriate ratio but of any magnitude. In practice, the conditions compatible with the homogeneous form of the equations are never achieved because of the inevitable departure from theoretical alinements and the presence of other small disturbances. For example, visualize equation (36) as being nonhomogeneous, that is, as having an infinitesimal right-hand member containing components independent of α and $1/R$. A solution of α_a and $1/R$ is then obtainable by Cramer's rule which will show that $\alpha_a \to \infty$ and $1/R \to \infty$ as the determinant of the left-hand side of the equation approaches zero.

Under extreme maneuvers implied by infinite values of α_a and $1/R$, it is obvious that structural failure and mission loss would result for the distinct combination of parameters when $q = q_{div}$. The divergence dynamic pressure thus defines the boundary between convergent and divergent performance.

Related Modal Characteristics

The coefficients A_1, A_2, B_1, and B_2 are those associated with the characteristic value q that satisfies equation (37) for the A and B solutions and when substituted into equation (36) will yield the applicable ratio of α_a to $1/R$. By normalizing on $1/R$ or α_a as desired, the initial value of α_a in terms of an assumed $1/R$ value may be determined. With initial values of α_a and $1/R$, a complete solution at all stations is then obtained by using equation (26). Such a solution yields the normalized moments, shear forces, and first derivative with respect to x of each variable compatible with the q_{div} solution. Thus, the solutions for the variables V, α, M, and their derivatives are essentially modal functions of the system by virtue of their dependency on an assumed flight-path curvature $1/R$.

Relationship Across Discontinuities

In order to accommodate discontinuous functions in the form of input and output characteristics, a set of relationships across points of discontinuity is established. These relationships are obtained by evaluating the recurrence formula given by equation (26) for $\Delta x_n = 0$. Consider equation (26) where the evaluations of $\mathbf{X}$ at stations n and n+1 correspond, respectively, to the solutions aft (-) and forward (+) of a discontinuity. Evaluation of equation (26) for $\Delta x_n = 0$ yields

$$\left\{X_{(+)}\right\} = \begin{Bmatrix} V'_{(+)} \\ V_{(+)} \\ \alpha'_{(+)} \\ \alpha_{(+)} \\ M'_{(+)} \\ M_{(+)} \\ (1/R)'_{(+)} \\ (1/R)_{(+)} \end{Bmatrix} = \begin{bmatrix} 0 & 0 & 0 & \left(S\frac{dC_{L_\alpha}}{dx}\right)_{(+)}q & 0 & 0 & 0 & -m_{(+)}u^2 \\ 0 & 1 & 0 & 0 & 0 & 0 & 0 & 0 \\ 0 & 0 & 0 & 0 & 0 & \left(\frac{1}{EI}\right)_{(+)} & 0 & -1 \\ 0 & 0 & 0 & 1 & 0 & 0 & 0 & 0 \\ 0 & 1 & 0 & P_{(+)} - \left(Sh\frac{d\overset{*}{C}_{M_\alpha}}{dx}\right)_{(+)}q & 0 & 0 & 0 & P_{(+)}x_{(+)} \\ 0 & 0 & 0 & 0 & 0 & 1 & 0 & 0 \\ 0 & 0 & 0 & 0 & 0 & 0 & 0 & 0 \\ 0 & 0 & 0 & 0 & 0 & 0 & 0 & 1 \end{bmatrix} \begin{Bmatrix} V'_{(-)} \\ V_{(-)} \\ \alpha'_{(-)} \\ \alpha_{(-)} \\ M'_{(-)} \\ M_{(-)} \\ (1/R)'_{(-)} \\ (1/R)_{(-)} \end{Bmatrix} \tag{38}$$

Equation (38) requires no additional programing since it automatically results from equation (26) by setting $\Delta x_n = 0$. The variables V, α, M, 1/R, and (1/R)' are seen to be continuous across the discontinuities as would normally be expected from physical considerations, whereas V', α', and M' are revealed as discontinuous functions.

DISCUSSION

In the preceding section the computational equations, integration technique, recurrence solution, boundary conditions, and stability equation have been developed. In addition, the modal nature of the solution for the variables was discussed and the necessary relationships for treatment of discontinuous functions were provided. This section is

devoted to the discussion of the numerical method of solution, the stability boundary q_{div}, results of comparative analyses, and the significance of secondary influences on aeroelastic divergence. Other topics discussed in this section include the stability criteria for acceptable design, the character and quality of required input data, and detailed output data obtained from the application of the method to a typical research vehicle. In addition, the results of parameter studies of the principal factors that influence divergence behavior serve to reveal some of the corrective measures that may be used to avoid divergence.

Numerical Solution

Several important considerations of the method in regard to solution procedures and some aspects of the digital computer program are discussed next.

Solving for the dynamic pressure of divergence.- The divergence dynamic pressure is mathematically obtained as the characteristic value of q that will satisfy equation (37). Equation (37) is seen to be of the form

$$f(q) = 0$$

which is solved by a trial and error procedure.

Acceptable results have been obtained by repeated trial solutions for $f(q)$ in which the trial value of q is successively increased by an increment of Δq until a sign change is indicated. This condition can be stated mathematically as

$$\frac{f\left(q^{n+1}\right)}{f\left(q^{n}\right)} < 0$$

where q^n is the nth trial value. Once the sign change is detected, an iteration procedure can be used to narrow the trial intervals of q until the difference between successive values is less than the desired tolerance so that $f(q) \approx 0$.

Integration intervals.- The basic differential equations given by equation (16) are of first order. Integration is performed on all variables by assuming linear variations in their first derivatives as required by equations (18) to (21a). In keeping with this assumption, the interval between all stations Δx must be suitably small. Computational accuracy studies have indicated that adequate results are normally obtained by describing all points of discontinuity in the input functions and by using a maximum Δx interval not exceeding 1/100 of the overall vehicle length. Where radical variations in the input functions occur, additional stations should be included to describe adequately such variations. Extensive experience with this method has shown that no impractical conditions arise when input-system characteristics are entered for as many as 400 intervals. Frequently, such a detailed description of input data is desirable for a multistage structure involving many discontinuities.

Computer time.- Efficient programing to minimize computer time is an important consideration for a problem of this scope. Improper programing may yield costly data as a result of lengthy computing times. Some considerations for minimizing computer time are set forth here.

The programing of the expanded form of equation (26) through the use of equations (28), (29), and (30) greatly reduces machine time in comparison with a program that requires the matrix operations of equation (26a) to be performed by the machine internally. Also, extreme and unmerited accuracy requirements on the solution for q_{div} to satisfy equation (37) increase machine time.

Another important consideration for reducing machine time is a realistic assessment of the accuracy requirements for satisfying upper boundary conditions. For example, V_l and M_l are zero for the free-free case, but achieving such absolute conditions on a digital computer is quite difficult if not impossible. Finite boundary values that are a fraction of 1 percent of the maximum value of their respective functions over the entire length $x_a \leqq x \leqq x_l$ are readily obtainable and should be accepted.

Dynamic Pressure of Divergence as a Measure of Stability

The significance of the solution for the divergence dynamic pressure and its use as a criterion for evaluating the aeroelastic stability of unguided launch vehicles are discussed briefly in the following paragraphs.

Significance.- The elements in the β matrix of equations (16) and (17) are dependent upon a particular altitude, Mach number, and flight time. In general, the divergence dynamic pressure obtained from equation (37) will be different from the nominal flight dynamic pressure. As pointed out by Alley and Gerringer in reference 3, the use of the difference between the divergence dynamic pressure and the nominal flight dynamic pressure as an indication of a stability margin does not require any further definition as to the probable altitude, Mach number, and time at which the hypothetical q_{div} could be obtained. Since the solution for q_{div} is implicit, the margin of stability based on dynamic pressure alone is associated with the constraint that all other pertinent parameters affecting the solution be held invariant.

Theoretical prediction of flight divergence failures: Since the computed dynamic pressure is incompatible with the actual trajectory employed for each analysis, a rigorous procedure is required if the objective is to predict the actual flight condition at which aeroelastic divergence will occur. If it is assumed that such a condition can occur along the trajectory, it is necessary to iterate for a number of solutions of equation (37). This procedure requires the input of new vehicle and trajectory characteristics associated with preceding estimates of q_{div} until the solution converges to a specified accuracy.

Such a solution will yield a dynamic pressure compatible with the time, altitude, velocity, mass, and aerodynamic characteristics for which it was obtained. Iteration for solutions of q_{div} is therefore desirable in attempting to correlate theoretical predictions with actual cases of aeroelastic divergence failures.

Stability criteria.- It is proposed in reference 3 that for a significantly flexible vehicle, an adequate margin against divergence can be assured by maintaining a constraint on q/q_{div}. The constraint is seen to be a necessary but not sufficient condition for vehicle stability. For flexible vehicle the constraint on q/q_{div} is the controlling criterion, but for highly rigid vehicles it is insufficient. For extremely stiff structures which might have rigid-body static margins near zero, a large margin against divergence may be indicated by a value of q/q_{div} near zero. The near-zero static margin is obviously undesirable in view of further reductions that might occur because of inaccuracies in aerodynamic and mass distribution and in view of the necessity of maintaining adequate frequency-response characteristics. Hence, in reference 3 the following three criteria were proposed for assuring adequate stability for vehicles within the extremes of flexibility and rigidity:

$$\frac{q}{q_{div}} \leqq 0.5$$

$$x_{sm,rig} \geqq D_{max}$$

$$x_{sm,rig} \geqq \frac{L}{15}$$

Should the analyst desire to adhere strictly to the static-margin criterion as a measure of stability, it is necessary to consider the degeneration in static margin due to aeroelasticity. Reference 3 provides a means for obtaining a generalized static margin for flexible vehicles that is analogous to the traditional rigid-body criterion but accounts for aeroelastic effects.

Comparative Numerical Solutions for the Dynamic Pressure of Divergence

Solutions for the divergence dynamic pressure of a flight-proven, two-stage, unguided Nike-Apache research vehicle were compared with those obtained for the same vehicle by the discrete element matrix method of reference 3. The summarized numerical results for q_{div} are presented in table I at four flight conditions. The input data used in the study were obtained from identical sources. The secondary influences of thrust and aerodynamic crossflow were excluded from the finite-difference recurrence analysis in order to obtain a valid comparison with the method of reference 3, which does not incorporate these effects.

TABLE I.- COMPARISON OF DIVERGENCE DYNAMIC PRESSURES FOR A NIKE-APACHE RESEARCH VEHICLE

Mach number	Divergence dynamic pressure, q_{div}			
	Finite-difference recurrence method		Discrete-element method of ref. 3	
	lbf/in^2	kN/m^2	lbf/in^2	kN/m^2
0	382.2	2 635.2	383.7	2 645.5
2.75	664.7	4 582.9	662.1	4 565.0
1.75	887.2	6 117.0	900.9	6 211.5
5.5	2014.2	13 887.4	1901.0	13 107.0

The results given in table I show good overall agreement between the divergence dynamic pressures computed by the two different methods.

Secondary Influences

The secondary influences of thrust and aerodynamic crossflow are of interest in the aeroelastic divergence analysis. The analytical method presented herein conveniently accommodates these terms in the equations that simulate divergent behavior.

The thrust tends to be a destabilizing factor since it introduces column buckling action, which contributes to vehicle deformation. The effect of column bending due to thrust is generally small in comparison with the bending induced by the transverse aerodynamic and inertial forces. However, when the thrust-mass ratio of the vehicle is very high, the thrust could have a significant influence on aeroelastic stability.

Aerodynamic crossflow induced by the angular velocities of the vehicle is found to be a stabilizing influence. This influence can be seen from equations (6) and (10), where x/R is the contribution to α due to the velocity crossflow effect. The term x/R serves to decrease the local angle of incidence which, in turn, reduces the magnitude of the aerodynamic lift forces.

Typical results of an investigation to determine the relative effects of thrust and aerodynamic crossflow on the divergence dynamic pressure for a typical high-performance research vehicle are illustrated in figure 2. The curves of figure 2 show the variation in $q_{div}/q_{div,o}$ with Mach number. The lower curve of figure 2 indicates that thrust is a destabilizing factor. The stabilizing influence of aerodynamic crossflow for the particular vehicle is illustrated by the upper dashed curve. Also note that the stabilizing effect of aerodynamic crossflow decreases with increase in Mach number since the crossflow term is inversely proportional to the vehicle velocity.

In general, comparative studies made by the author on a number of unguided launch vehicles have revealed that for most typical research vehicle designs the aforementioned secondary influences do not have a significant effect on stability.

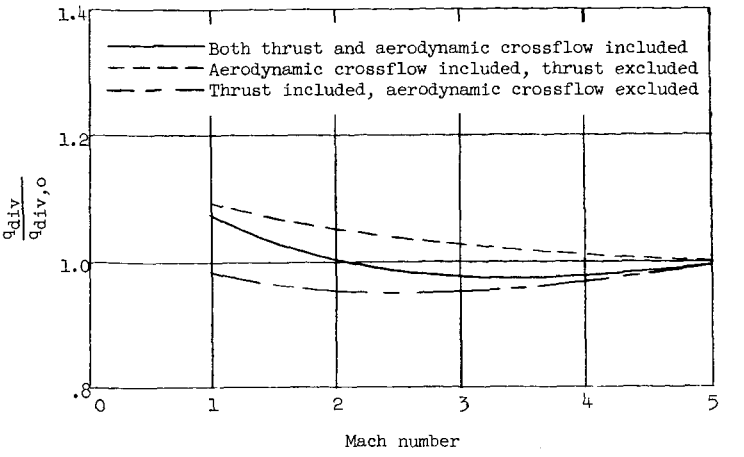

Figure 2.- Secondary effects of thrust and aerodynamic crossflow on divergence dynamic pressure.

Numerical Application

The successful use of the analytical procedure presented in this paper is dependent upon the adequate representation of the vehicle stiffness, mass, and aerodynamic characteristics, as well as a knowledge of the pertinent trajectory parameters. In this section, typical input data necessary to an analysis are furnished and some important considerations in obtaining such input data are discussed. In addition, output data for an example analysis are presented along with comments on the results.

Input characteristics.- The graphs of necessary input functions included herein serve to illustrate the capability and advantages of the proposed method in accommodating highly descriptive and discontinuous input characteristics. All points of discontinuity in the input functions are established in the analysis to provide adequate representation over radical variations.

Stiffness data: Flexural stiffness coefficients computed for the conceptual NASA research vehicle SV-144 are given in table II and are shown graphically in figure 3. Note that these data provide a highly descriptive representation of the variational stiffness level of the composite cylindrical shell-like structure. The discontinuities evident in figure 3 are accounted for in table II by recording both quantities for their common x/L value.

The results obtained from the aeroelastic divergence analysis are strongly dependent upon the quality of the EI data. The analyst must give careful consideration to the determination of load paths, and the use of equivalent stiffness quantities to provide for plate and shell deformations and for other flexibility considerations not treated by the elementary beam theory. For example,rotations of appreciable magnitude may occur at structural junctures. The inordinate behavior at structural joints normally defies rigorous analytical techniques, but empirical methods, such as those of reference 8, can be used. The local joint constants κ_u given in reference 8 can be incorporated into the

TABLE II.- FLEXURAL STIFFNESS DISTRIBUTION FOR THE CONCEPTUAL SV-144 RESEARCH VEHICLE[a]

$\left[(EI)_{ref} = 100 \times 10^9 \text{ lbf-in}^2 \quad (0.287 \times 10^9 \text{ N-m}^2)\right.$
$\left.L = 825.95 \text{ in.} \quad (20.98 \text{ m})\right]$

$\frac{x}{L}$	$\frac{EI}{(EI)_{ref}}$	$\frac{x}{L}$	$\frac{EI}{(EI)_{ref}}$	$\frac{x}{L}$	$\frac{EI}{(EI)_{ref}}$
-0.0202	1.1857	0.4762	0.2912	0.8629	0.0643
0	1.1857	.4762	.2912	.8629	.0399
.0216	1.1857	.4780	.2881	.8666	.0399
.0216	.2016	.4780	.1157	.8666	.0677
.0252	.2016	.4817	.1157	.8725	.0513
.0252	1.3434	.4817	.8957	.8802	.0345
.0284	1.3434	.6415	.8957	.8862	.0249
.0284	2.9979	.6415	.1153	.8862	.0049
.0502	2.9979	.6451	.1153	.8910	.0049
.0502	.7855	.6451	.2806	.8910	.0044
.2107	.7855	.6560	.2806	.8926	.0050
.2137	1.5101	.6560	.1006	.8937	.0052
.2167	.7855	.6596	.1006	.8992	.0069
.3744	.7855	.6596	.2663	.9060	.0100
.3744	2.998	.6699	.1851	.9121	.0137
.3962	2.998	.6820	.1141	.9181	.0172
.3962	1.3434	.6941	.0641	.9242	.0182
.4005	1.3434	.7002	.0458	.9279	.0169
.4005	.1928	.7020	.0413	.9307	.0163
.4042	.1928	.7020	.0239	.9325	.0142
.4042	.7740	.7068	.0239	.9325	.0293
.4211	.7740	.7184	.0534	.9363	.0251
.4211	.1639	.8401	.0534	.9423	.0193
.4248	.1639	.8425	.0632	.9484	.0145
.4248	.3877	.8425	.0705	.9543	.0105
.4278	.3815	.8462	.1306	.9629	.0063
.4399	.3574	.8462	.0161	.9629	.0644
.4472	.3717	.8498	.0161	.9690	.0416
.4520	.3343	.8498	.0246	.9726	.031
.4624	.3151	.8536	.0312	.9798	0
.4641	.3123	.8596	.0489		

[a]Points of discontinuity in the $EI/(EI)_{ref}$ function are recorded for their common x/L values. The first and repeated x/L quantities correspond to the values of the $EI/(EI)_{ref}$ function on the (-) and (+) sides, respectively, of the discontinuity.

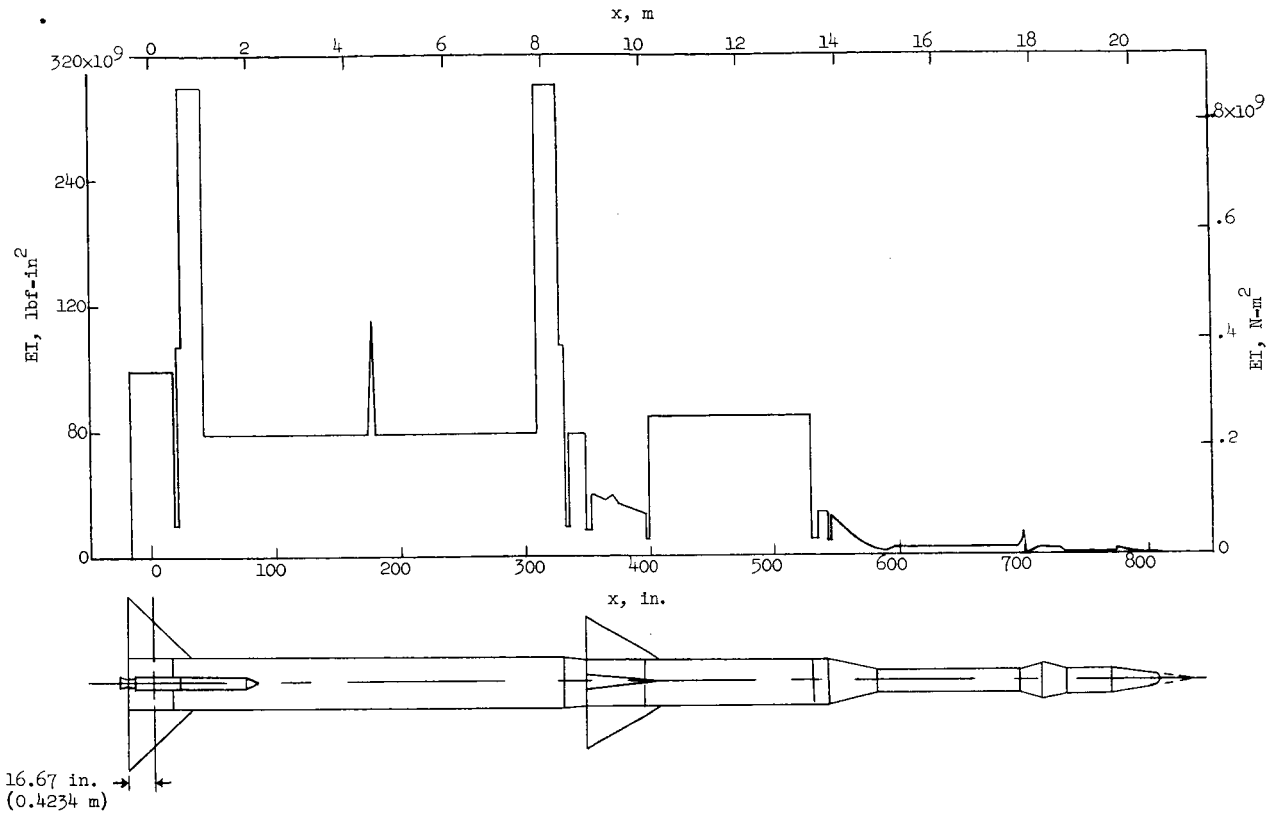

Figure 3.- Flexural-stiffness-coefficient distribution for the conceptual SV-144 research vehicle.

analysis by making an alteration to the EI distribution over an arbitrary short interval through the use of the following approximation:

$$(EI)_e = \frac{\Delta x}{\kappa_u + \int_x^{x+\Delta x} \frac{1}{EI}\, dx} \tag{39}$$

The relationship of equation (39) is based on the assumption that $(EI)_e$ is constant over the joint interval Δx, which must be small although arbitrary. The interval Δx is frequently taken between 2 and 5 percent of the appropriate stage lengths. The joint-rotation information of reference 8 was used in the applied analysis of the SV-144 to approximate stiffness distributions across structural joints.

The use of certain materials such as fiber glass in the structural design of a vehicle may introduce questionable stiffness characteristics. In addition, where structural heating is severe, the analyst should give adequate consideration to problems of stiffness degeneration.

Mass data: The tabulated mass distributions for the SV-144 research vehicle just prior to launch are furnished in table III. These data (along with the first-stage burnout distribution) are illustrated graphically in figure 4. The continuous mass inputs allow a highly descriptive representation of the variable mass characteristics and an equally

TABLE III.- MASS DISTRIBUTION PRIOR TO LAUNCH FOR THE CONCEPTUAL SV-144 RESEARCH VEHICLE[a]

$$\left[m_{ref} = 1.0 \frac{lbf\text{-}sec^2}{in^2} \quad \left(6894.7572 \frac{N\text{-}sec^2}{m^2} \right) \right]$$

$$L = 825.95 \text{ in.} \quad (20.98 \text{ m})$$

$\frac{x}{L}$	$\frac{m}{m_{ref}}$	$\frac{x}{L}$	$\frac{m}{m_{ref}}$	$\frac{x}{L}$	$\frac{m}{m_{ref}}$
-0.0202	0.0190	0.4762	0.0229	0.8498	0.0016
-.0081	.0190	.4798	.0229	.8536	.0017
0	.1384	.4798	.1624	.8596	.0019
.0234	.1384	.5004	.1982	.8629	.0297
.0234	.3124	.5125	.1462	.8647	.0449
.0284	.3124	.6433	.1462	.8666	.0355
.0393	.3354	.6433	.0067	.8725	.0048
.0502	.2160	.6451	.0072	.8802	.0051
.0502	.1873	.6560	.0102	.8862	.0166
.2107	.1873	.6578	.0170	.8880	.0202
.2137	.1964	.6596	.0165	.8880	.0473
.2167	.1873	.6699	.0071	.8910	.0473
.3744	.1873	.6820	.0166	.8937	.0286
.3744	.2160	.6941	.0031	.8992	.0403
.3962	.2160	.7002	.0028	.9060	.0403
.3962	.1929	.7020	.0027	.9121	.0704
.4024	.1929	.7038	.0026	.9181	.0403
.4024	.0097	.7038	.0383	.9325	.0403
.4157	.0097	.7068	.0362	.9325	.0018
.4211	.0467	.7184	.0621	.9423	.0016
.4229	.0589	.7305	.0362	.9484	.0166
.4229	.0542	.8401	.0362	.9545	.0010
.4278	.0542	.8425	.0335	.9629	.0009
.4399	.0067	.8425	.0339	.9629	.0068
.4472	.0297	.8462	.0295	.9690	.0059
.4520	.0341	.8470	.0285	.9726	.0053
.4641	.0230	.8470	.0591	.9798	0

[a]Points of discontinuity in the m/m_{ref} function are recorded for their common x/L values. The first and repeated x/L quantities correspond to the values of the m/m_{ref} function on the (-) and (+) sides, respectively, of the discontinuity.

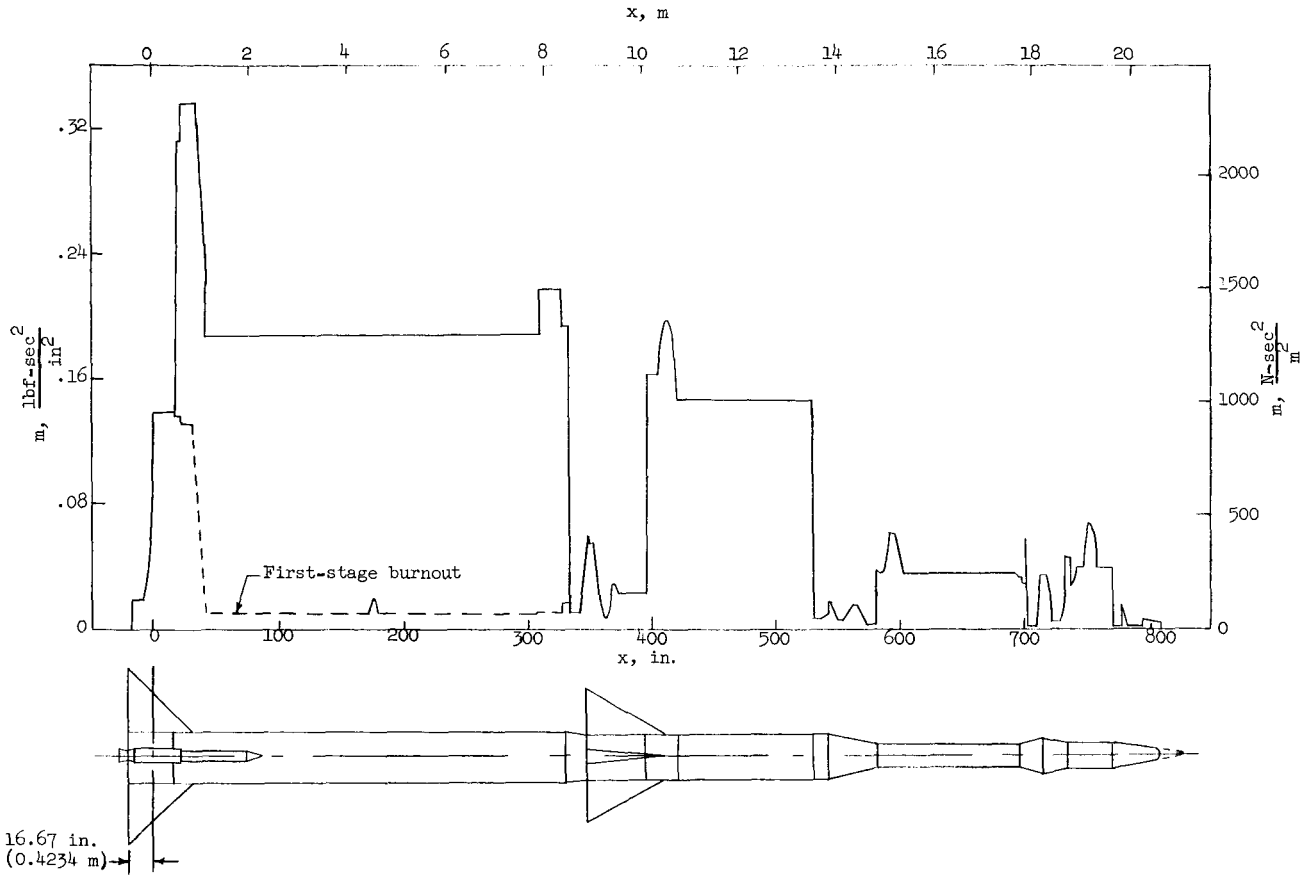

Figure 4.- Mass distribution for the conceptual SV-144 research vehicle.

descriptive representation of the inertial loads on the system. Frequently, the analyst must consider intermediate mass values of the aforementioned distributions as well as other stages of the configuration.

Aerodynamic data: The divergence dynamic pressure is dependent on the aerodynamic distributions as well as the stiffness and mass characteristics. Consequently, an accurate description of the aerodynamic characteristics is desirable for the comprehensive divergence analysis. The computed fin lift data as a function of Mach number for the SV-144 research vehicle are presented in figure 5. These fin-lift coefficient derivatives were obtained through the use of methods set forth in reference 9. Coefficients are provided for the total fin area of two panels in one plane and include downwash effects from forward fins as well as wing-body carryover effects. The analyst must consider downwash effects because the effectiveness of the aft lifting surface can be drastically reduced by downwash interference from forward lifting surfaces. Interdigitation of forward fins can, in some cases, partially reduce undesirable fin downwash effects.

The analyst must also consider the loss of fin effectiveness at high altitudes resulting from flow separation due to interference from the rocket-exhaust jet plume. Reports on the effects of jet pluming on stability are available in references 10 and 11.

Distributed body aerodynamic lift-force derivatives valid at small angles of attack for the SV-144 research vehicle at Mach numbers of 3.5 and 5 are illustrated in the graphs of figure 6. From these curves, the aerodynamic loading along the body of the vehicle would be obtained as the product of the aerodynamic loading function $S\frac{dC_{L_\alpha}}{dx}$, the local angle of attack, and the free-stream dynamic pressure. The data of figure 6 were generated from the empirical data compiled in reference 12 which are very useful for the flexible-vehicle analysis utilizing distributed aerodynamic lift-force data.

Several theoretical methods are available for determining the distributed aerodynamic characteristics for slender bodies. These methods include the second-order perturbation theory for inclined bodies of revolution of reference 13, the generalized shock-expansion method of reference 14, and the linearized theory for bodies of revolution discussed in reference 15.

Trajectory data: Various parameters such as velocity, Mach number, thrust, and dynamic pressure, obtained from the computed flight trajectory, are necessary inputs to the divergence analysis. Time histories of the trajectory characteristics for the conceptual SV-144 research vehicle are provided in figure 7. Case studies are normally established at ignition and at burnout of each stage, at Mach 1, at time of minimum static margin, at discontinuous points such as times prior to and subsequent to stage separation, and at times of maximum dynamic pressure. Of these, the case at maximum dynamic pressure is usually the most significant. Also, multistage vehicles attaining hypersonic velocities may encounter critical conditions during upper stages of flight; thus, a complete time-history study for all stages of flight is desirable.

The analyst should also consider the dispersion possibilities of launching below the minimal launch angle called for in the programed trajectory. Reductions in launch angle for the unguided vehicle are coupled with increases in flight dynamic pressure. A complete design evaluation should account for standard low deviations in the launch angle, particularly in cases of marginal aeroelastic stability.

Output characteristics.- The significant output data obtained from the divergence analysis consist of the stability boundary q_{div} as well as the numerical solution for the $\{X\}$ variables at each station along the vehicle.

Stability index q/q_{div}: As previously mentioned, the dynamic pressure ratio obtained from the analysis is used to evaluate the aeroelastic stability of the launch vehicle. The timewise variation in the computed q/q_{div} index during the first-stage flight

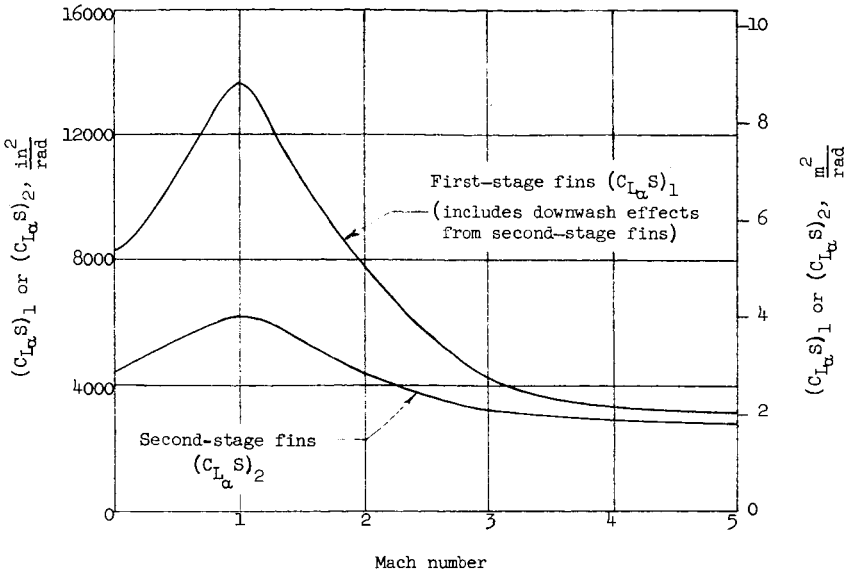

Figure 5.- Fin lift data for the conceptual SV-144 research vehicle. Valid for two panels in one plane.

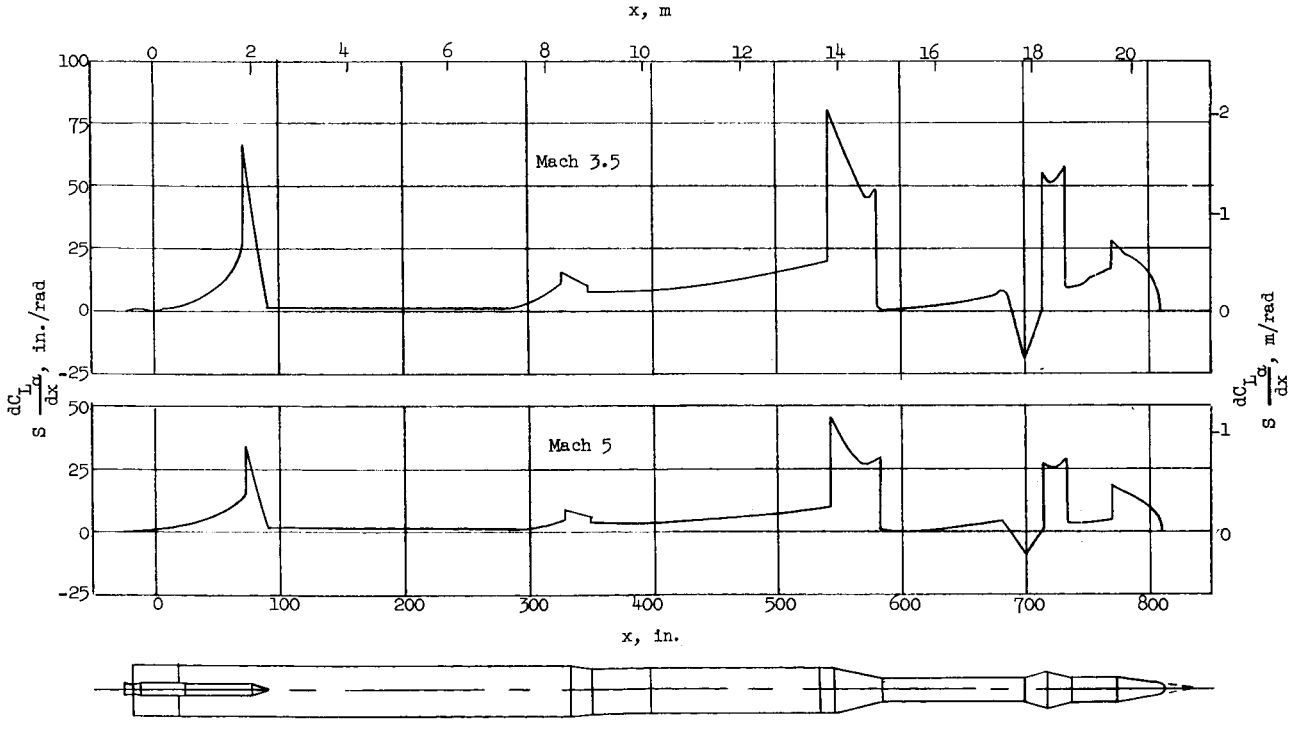

Figure 6.- Distributed body aerodynamic lift-force-coefficient slopes for the conceptual SV-144 research vehicle at Mach numbers of 3.5 and 5.

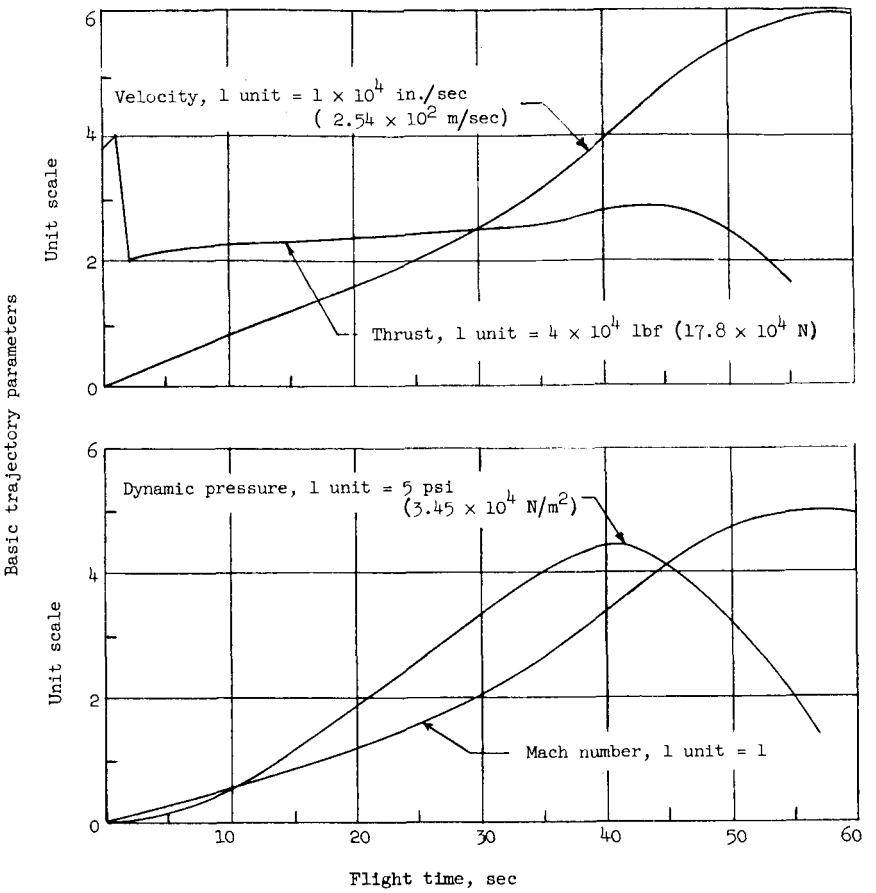

Figure 7.- Basic trajectory parameters for the conceptual SV-144 research vehicle.

for the conceptual SV-144 research vehicle is given in figure 8. The computed peak value of q/q_{div} is 0.19 and occurs at $t = 42$ seconds at a Mach number of 3.5. A maximum value of 0.19 for q/q_{div} is conservative in view of the aforementioned criterion of $q/q_{div} \leq 0.5$ and indicates acceptable compatibility between the static aerodynamic, structural, and trajectory characteristics of the system. When $q/q_{div} > 0.5$ for design conditions, the vehicle may be subjected to large aeroelastic load magnifications and rapid stability degeneration. Stability degeneration of designs having $q/q_{div} > 0.5$ is investigated in reference 3 and is shown in parameter studies in subsequent sections of this paper.

Modal functions: The numerical solution for the variables V', V, α', α, M', and M is obtainable from equation (26). As previously discussed in the section entitled "Analysis," these variables are the modal characteristics associated with the characteristic value q_{div}. The graphs shown in figures 9 to 11 typify the output for the solutions to the system variables that are associated with the divergence mode. These data are applicable to the SV-144 research vehicle at maximum dynamic pressure (t = 42 sec).

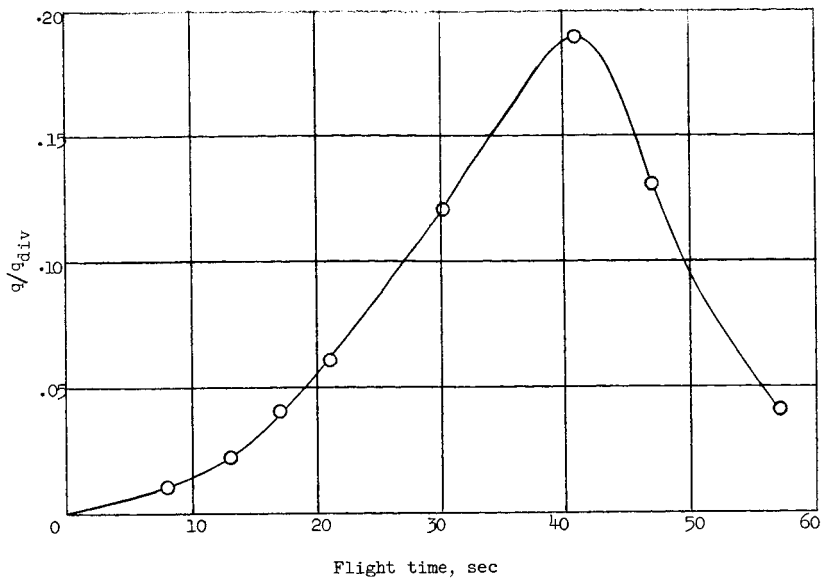

Figure 8.- Variation of the computed stability index q/q_{div} with flight time for the conceptual SV-144 research vehicle.

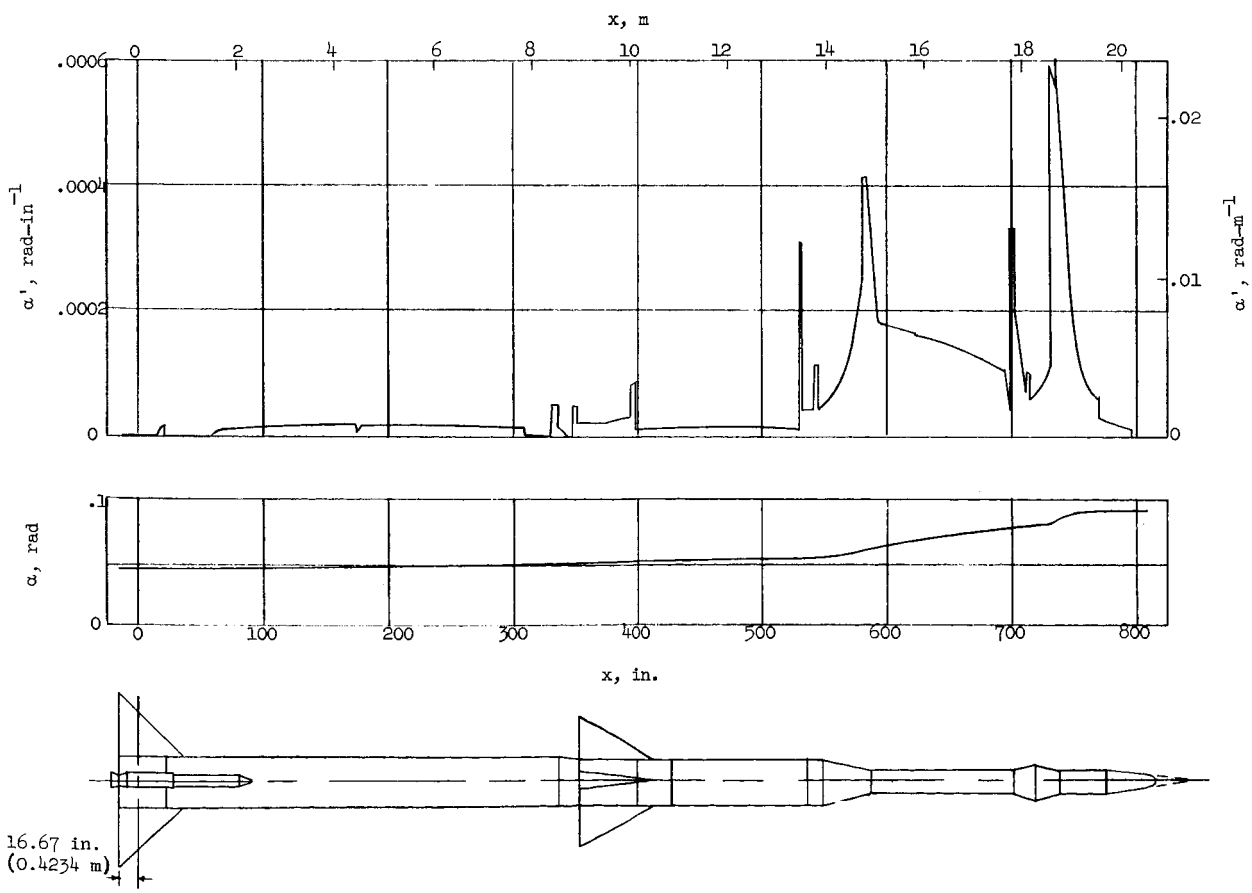

Figure 9.- Modal characteristics α and α' associated with the divergence dynamic pressure at a Mach number of 3.5 for the conceptual SV-144 research vehicle.

The divergence attitude of the deformed vehicle is indicated by the plots of α' and α. Also, the distributed loading functions on the vehicle are given by the graphs of V', V, M', and M. Note that the α function in figure 9 is continuous and appears as would generally be expected; however, α' is seen to be highly discontinuous by virtue of its dependency upon the EI function.

The M' function, which is generally equal to V when simple beam theory loading is assumed, departs herein by virtue of the inclusion of the axial load components. These components result from the aerodynamic, thrust, and induced inertial column loadings, as can be seen from equation (13). The M' function of figure 10 and the V function of figure 11 are therefore not identical.

The V' function given in figure 11 is normally observed as the load per unit length from the elementary beam theory. The V' function obtained from the recurrence solution gives similar results. This function consists of the inertial and aerodynamic transverse force distributions defined by equation (12).

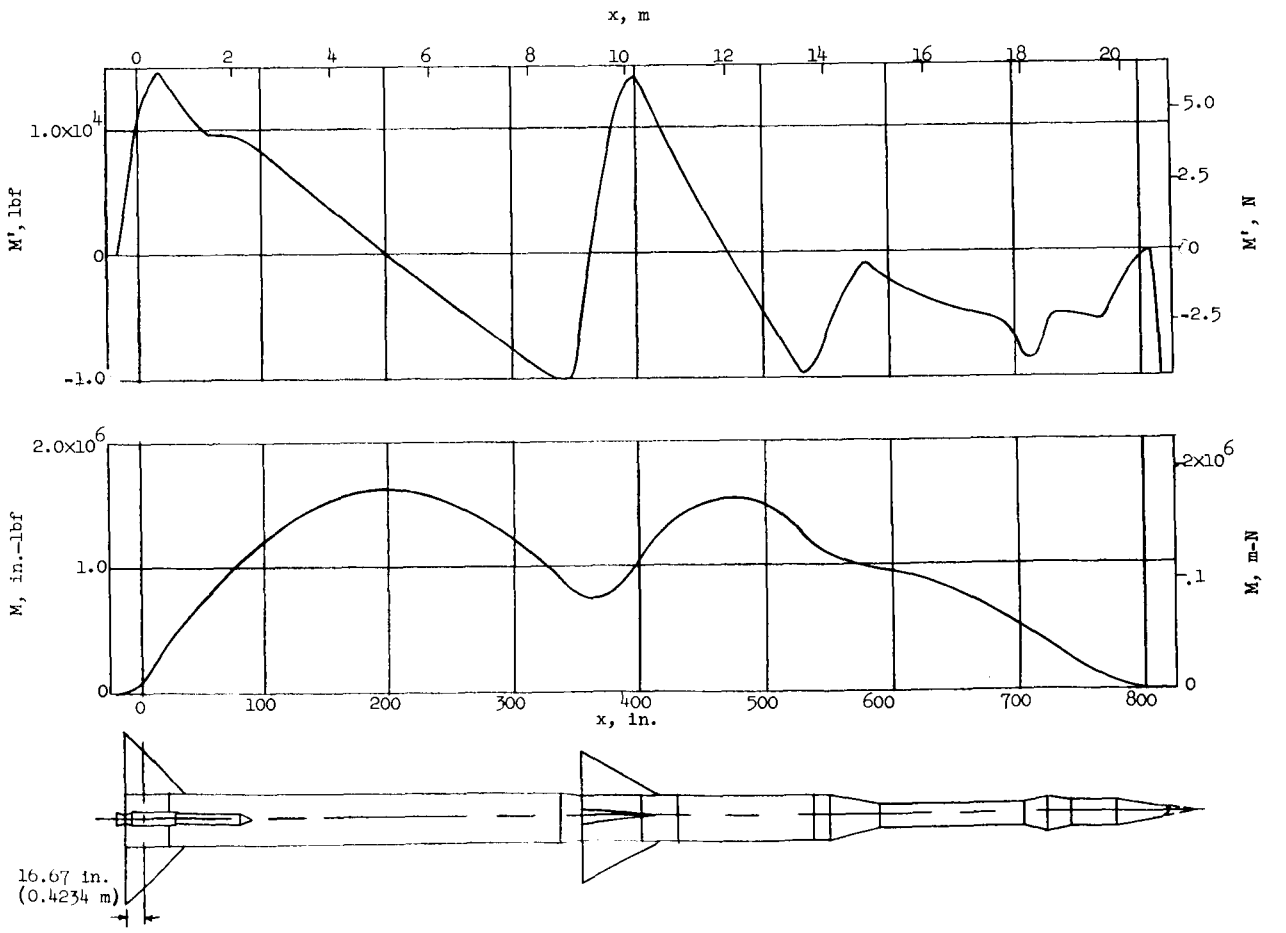

Figure 10.- Modal characteristics M and M' associated with the divergence dynamic pressure at a Mach number of 3.5 for the conceptual SV-144 research vehicle.

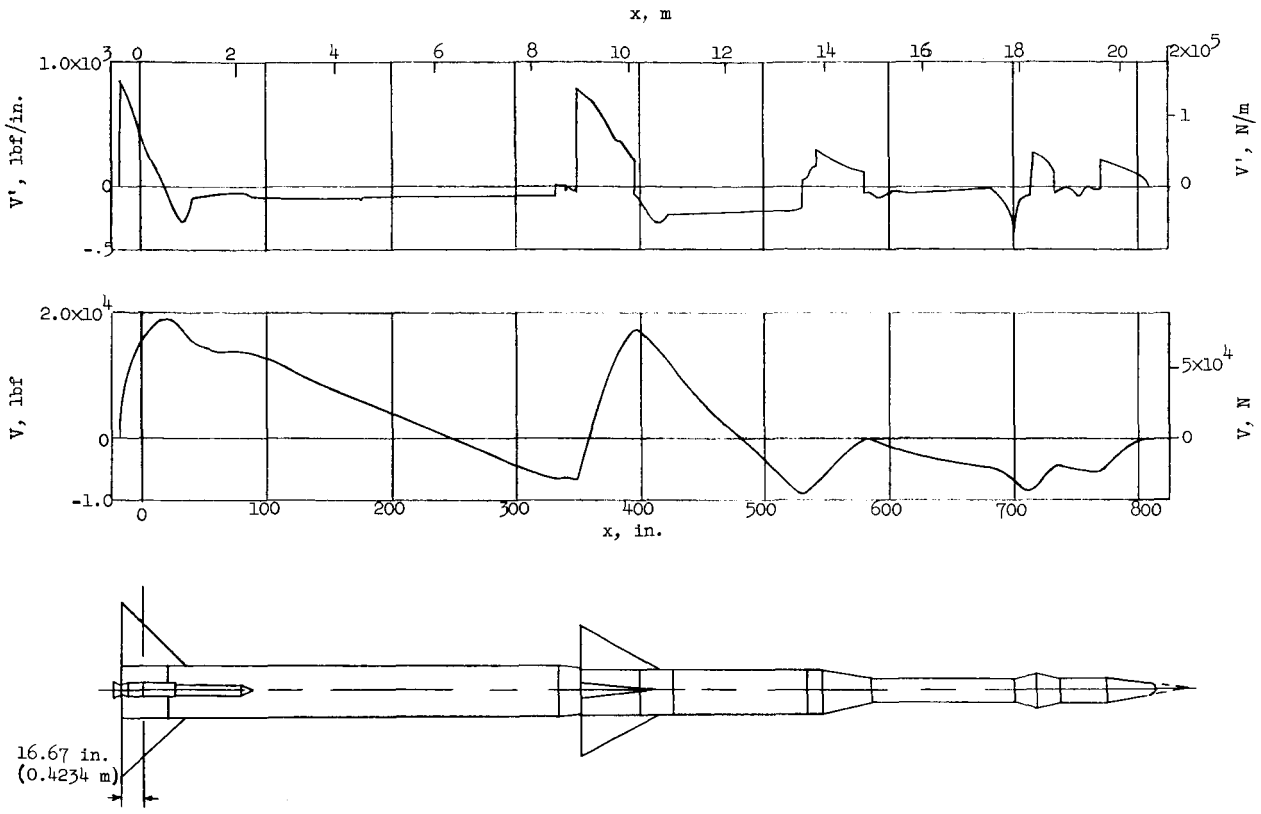

Figure 11.- Modal characteristics V and V' associated with the divergence dynamic pressure at a Mach number of 3.5 for the conceptual SV-144 research vehicle.

A characteristic divergence mode shape for the SV-144 research vehicle constrained to a curvilinear flight path is illustrated in figure 12. This mode shape is the fundamental or zero-frequency mode of divergence and is associated with a normalized flight-path curvature of 0.1×10^{-5} inch^{-1} (0.254×10^{-7} m^{-1}). The divergence mode shape may be obtained from the analysis by substituting equation (10) into equation (6) and performing a numerical integration to obtain the displacement y that is associated with the divergence functions α_a and 1/R.

Remedial Measures

The analyst must be prepared to recommend changes that can bring critical or marginal designs within acceptable limits. The most expedient remedial measures are normally limited to aerodynamic changes, local stiffness corrections, and restrictions on the trajectory. In this section some effective ways of improving aeroelastic stability characteristics are illustrated by means of parameter studies and other analytical considerations.

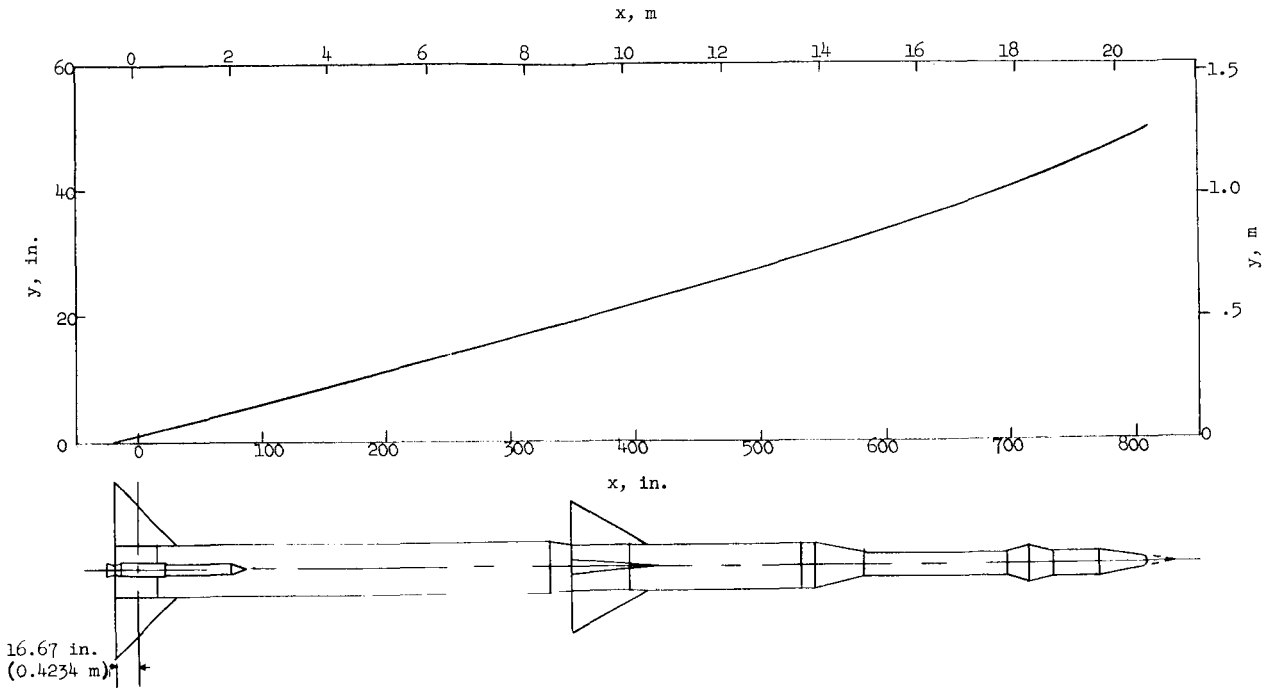

Figure 12.- Shape of the vehicle in the divergence mode; $\frac{1}{R} = 0.1 \times 10^{-5}$ inch^{-1} $\left(0.254 \times 10^{-7}\ \text{m}^{-1}\right)$.

Changes in aerodynamic characteristics.- Significant changes in the stability index q/q_{div} occur as a result of varying the aerodynamic lift effectiveness. These changes, shown in figure 13 and 14, are discussed in the following paragraphs.

First-stage fins: Changes in the q/q_{div} index due to variations in the first-stage-fin lift-coefficient derivative are presented in figure 13. The curves indicate that the stability index q/q_{div} can be improved by increases in the first-stage fin-lift effectiveness. However, it should be noted that only trivial gains can be accomplished in the regions where the slopes of the curves are low, and the improvement frequently may not justify the disadvantages of excessively large fins. An upper bound to fin size normally exists because of fin flutter characteristics, fin drag, and weight. When such limitations are encountered, the analyst must employ other corrective measures.

It is interesting to note that the findings for the SV-144 research vehicle indicate that the first-stage fins are more than adequate to satisfy the stability criterion and that the trajectory could be more nearly optimized by reducing the first-stage fin size and, consequently, the fin drag and weight. For example, based on the criterion of $q/q_{div} \leq 0.5$, a reduction in fin size of 30 percent, corresponding to a nominal fin lift ratio of 0.7, would still yield an acceptable value of $q/q_{div} = 0.4$. However, any fin lift reductions beyond this point would be undesirable because of the rapid degeneration in stability with small decrease in fin lift, which is indicated by the high slope of the curves.

From figure 13 it is apparent that q/q_{div} is highly sensitive to variations in the aerodynamic coefficient ratios between 0.6 and 0.7. If confidence is to be maintained in stability margins for designs falling in ranges where the curves are becoming vertically asymptotic, it is evident that accurate aerodynamic data are needed. In such cases, data such as those of figure 13 can be useful as justification for actual wind-tunnel measurements. However, for designs falling on the portions of the curve becoming horizontally asymptotic, accuracy of aerodynamic data becomes less important.

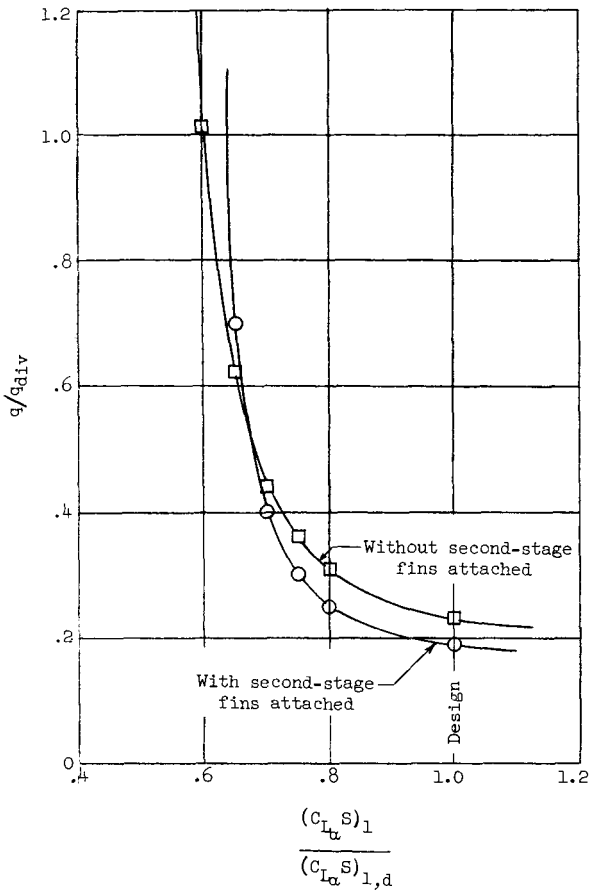

Figure 13.- Variation of q/q_{div} for various ratios of the first-stage nominal fin aerodynamic characteristics.

Interstage fins: The effect of second-stage-fin lift effectiveness on aeroelastic divergence for the SV-144 research vehicle can also be seen in figure 13. Observe from the lower curve that for first-stage-fin lift ratios less than 0.67, the second-stage fins produce the reverse of the normally expected trend, that is, the second-stage fins have a destabilizing effect. Recall that aeroelastic divergence becomes increasingly critical with decreasing static margin. In this case, the second-stage fins of the SV-144 research vehicle are located forward of the aerodynamic center of pressure during first-stage flight and therefore tend to reduce the static margin. However, for values of $(C_{L_\alpha}S)_1/(C_{L_\alpha}S)_{1,d}$ greater than 0.67, this disadvantage is outweighed by the advantage of providing a more uniform load-carrying system and thus reducing elastic deformations (that is, the second-stage fins act as an intermediate support for carrying inertia loads as the center of gravity moves forward). However, for fin lift ratios less than 0.67, the second-stage fins produce such radical changes in the aerodynamic center of pressure that the loss in static margin for stability outweighs the advantages of structural support.

In many cases, the margin against divergence may be improved by considering changes in interstage-fin lift characteristics. However, the analyst must again consider the problems that may accompany these changes, such as downwash effects, flutter boundaries, increased drag and weight, and severe reductions in static margin.

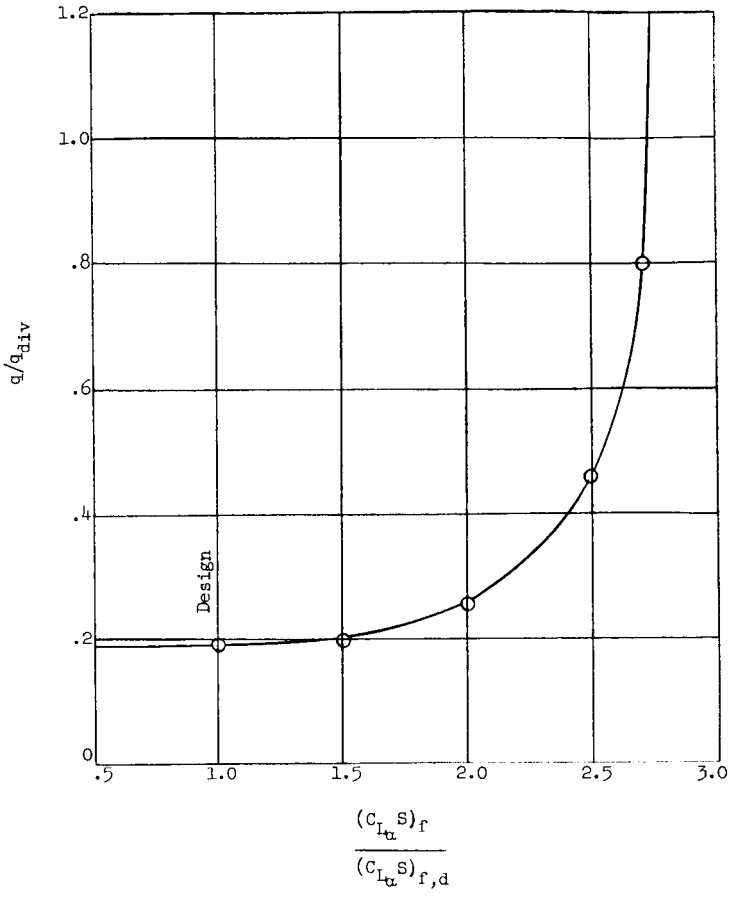

Figure 14.- Variation of stability index q/q_{div} for various ratios of nominal flare aerodynamic characteristics.

Forward lifting surfaces: A further effect of lift distributions on divergence is shown in figure 14. The curve illustrates changes in the q/q_{div} index with amplification of nominal lift distributions over the flare adapters (frustum) between the third and fourth stages and between the fourth stage and payload for the SV-144 research vehicle. Note that aerodynamic load magnifications in excess of 2.25 produce high slopes for the q/q_{div} curve, which indicate a rapid degeneration in stability. Similar results would be expected for increased lift over the nose or some other forward lifting surface, and the flare distributions of figure 14 are merely illustrative. In essence, the data indicate that high lift concentrations over the forward stages of the vehicle give rise to the aeroelastic divergence problem since the weight and stiffness functions in these areas are normally minimal due to vehicle performance requirements.

Structural stiffness improvements.- Increasing the structural rigidity of a vehicle is, of course, a primary consideration for improving aeroelastic design. Flexibility effects become increasingly important in the design of vehicles with large slenderness ratios.

The curves of figure 15 indicate the stability sensitivity of the specific vehicle with increased flexibility. The upper curve illustrates stability degeneration, as shown by the increased slope of the q/q_{div} curve, for stiffness ratios less than 0.4 for the upper three stages. Similar stiffness reductions over only the third and fourth stages have less effect on q/q_{div}, as would be expected. These curves illustrate the potential increase in q/q_{div} that could result with reductions in stiffness. For vehicle designs less conservative than the SV-144 research vehicle, radical changes in q/q_{div} ratios might frequently result with only moderate stiffness reductions.

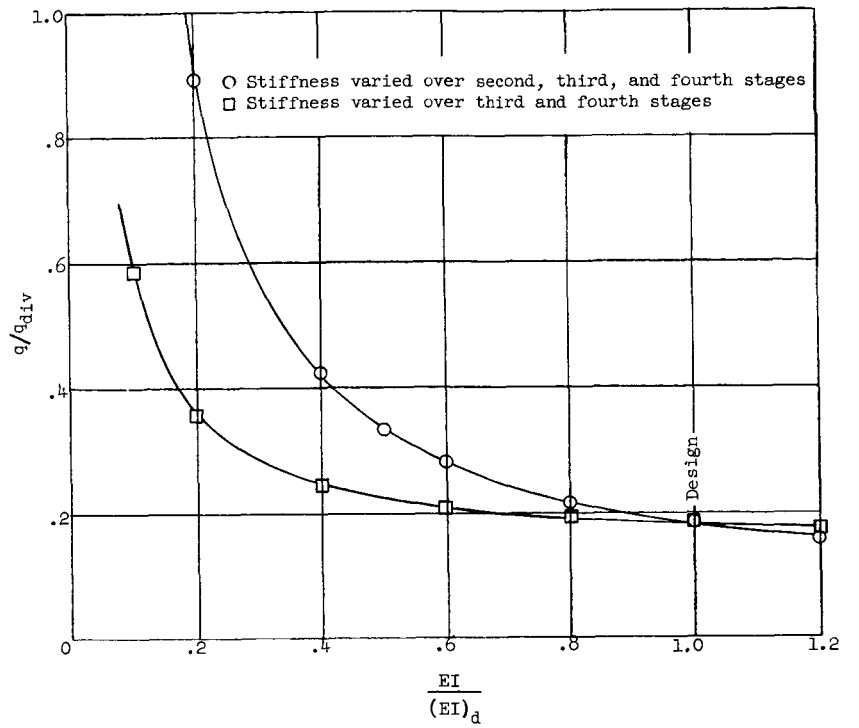

Figure 15.- Variation of stability index q/q_{div} for various ratios of nominal stiffness distributions for the upper stages of the conceptual SV-144 research vehicle.

The results of figure 15 indicate that divergence may be avoided by increasing the structural rigidity of the vehicle. This procedure is most effective when the slope of the q/q_{div} curve is high. In the regions where the slope of the q/q_{div} curve is low, the improvement may not justify the disadvantage of increased weight or additional structural design modification. When extreme local flexure is apparent from structural test observations or poor joint design is evident, structural redesign measures become practical and significant improvements can be made. The technique of improving the structural stiffness is often employed by the analyst in avoiding divergence problems. For example, Thomson (ref. 2) used this approach in an attempt to achieve successful flight by stiffening the second stage of a two-stage vehicle that was found to be divergent.

Alteration of mass characteristics.- Another procedure for avoiding divergence is to alter the mass characteristics in order to increase the static margin. By moving the center of gravity a significant distance forward of the aerodynamic center of pressure, a greater aerodynamic restoring moment is obtained. However, this procedure is generally prohibited because of adverse effects on performance, particularly during the upper stages of flight.

Changes in the flight trajectory.- Most remedial measures will alter the vehicle performance to some degree. However, in some cases the most expedient method for

avoiding divergence may be to reduce the maximum dynamic pressure. For vehicles that are not normally launched vertically, the dynamic pressure may be significantly reduced by increasing the launch angle. Also, the flight dynamic pressure may be lowered by reducing the thrust levels, by the prudent use of coast periods, and by the addition of ballast.

CONCLUDING REMARKS

A finite-difference recurrence method is presented for theoretically analyzing the aeroelastic divergence behavior of unguided, slender-body launch vehicles. The method has been found to be rapid, accurate, and economical for obtaining the numerical solution for the divergence dynamic pressure on digital computer systems.

Comparative studies show good agreement between the recurrence solution and a discrete element matrix method. The significance of the secondary influences of thrust and aerodynamic crossflow on the aeroelastic divergence behavior is investigated, and it is concluded that for most practical applications they can be ignored.

The analysis is applied to a typical research vehicle for which necessary input data and detailed output data are provided.

Prudent alterations to aerodynamic and stiffness characteristics are effective measures to bring marginally stable vehicles within the bounds of accepted stability criteria. Other effective remedial measures include ballasting and modifications to the flight trajectory.

Langley Research Center,
National Aeronautics and Space Administration,
Langley Station, Hampton, Va., October 19, 1966,
124-11-05-30-23.

APPENDIX

SUPERPOSITION OF BOUNDARY CONDITIONS AS APPLIED TO THE RECURRENCE SOLUTION

The validity of superposition in the theory of linear equations is readily realized for independent and additive treatment of nonhomogeneous terms; however, the validity of superposition of boundary conditions is not so clearly apparent. Since the method presented in this paper is based on superposition of the lower boundary conditions, it is important that the validity of this procedure be fully established.

The recurrence relationship for the homogeneous system is given by equation (26), repeated here for convenience:

$$\left\{X_{n+1}\right\} = \left[K_{n+1}\right]\left\{X_n\right\} \tag{A1}$$

At the lower boundary, where $n = a$ at $x = x_a$, equation (A1) becomes

$$\left\{X_{a+1}\right\} = \left[K_{a+1}\right]\left\{X_a\right\} \tag{A2}$$

The column matrix $\left\{X_a\right\}$ for the general case defines the lower boundary conditions dependent upon the values assigned to the variables V_a, α_a, M_a, and $1/R$. Thus, a general expression for the solution at the lower boundary can be written as

$$\left\{X_{n=a}\right\} = \alpha_a\left\{X_a\right\}_A + \frac{1}{R}\left\{X_a\right\}_B + V_a\left\{X_a\right\}_C + M_a\left\{X_a\right\}_D \tag{A3}$$

where the subscripts A, B, C, and D denote the form of the boundary-value vector X_a associated with the single unit values of α_a, $1/R$, V_a, and M_a, respectively. For example, the A solution for the general case applies for the unit boundary relationship where $\alpha_a = 1$ when $1/R = V_a = M_a = 0$. By separate substitution of the appropriate boundary relationships for the aforementioned solutions designated A to D in equation (16), the generalized lower boundary vectors are obtained as

$$\left\{X_a\right\}_A = \begin{Bmatrix} \left(S \frac{dC_{L_\alpha}}{dx}\right)_a q \\ 0 \\ 0 \\ 1 \\ P_a - \left(Sh \frac{dC^*_{M_\alpha}}{dx}\right)_a q \\ 0 \\ 0 \\ 0 \end{Bmatrix} \qquad \left\{X_a\right\}_B = \begin{Bmatrix} -m_a u^2 \\ 0 \\ -1 \\ 0 \\ P_a x_a \\ 0 \\ 0 \\ 1 \end{Bmatrix}$$

$$\left\{X_a\right\}_C = \begin{Bmatrix} 0 \\ 1 \\ 0 \\ 0 \\ 1 \\ 0 \\ 0 \\ 0 \end{Bmatrix} \qquad \left\{X_a\right\}_D = \begin{Bmatrix} 0 \\ 0 \\ \left(\frac{1}{EI}\right)_a \\ 0 \\ 0 \\ 1 \\ 0 \\ 0 \end{Bmatrix} \qquad \text{(A4)}$$

Substituting equation (A3) into equation (A2) gives

$$\left\{X_{a+1}\right\} = \left[K_{a+1}\right]\left\{\alpha_a \left\{X_a\right\}_A + \frac{1}{R}\left\{X_a\right\}_B + V_a \left\{X_a\right\}_C + M_a \left\{X_a\right\}_D\right\} \qquad \text{(A5)}$$

Equation (A5) will then provide the desired solution for the variables at $x = x_{a+1}$. For $n = a + 1$, equation (A1) becomes

$$\left\{X_{a+2}\right\} = \left[K_{a+2}\right]\left\{X_{a+1}\right\} \qquad \text{(A6)}$$

Substituting equation (A5) into equation (A6) yields

$$\left\{X_{a+2}\right\} = \left[K_{a+2}\right]\left[K_{a+1}\right]\left\{\alpha_a\left\{X_a\right\}_A + \frac{1}{R}\left\{X_a\right\}_B + V_a\left\{X_a\right\}_C + M_a\left\{X_a\right\}_D\right\} \tag{A7}$$

It can be seen that if this process is repeated the recurrence equation will take the form

$$\left\{X_{n+1}\right\} = \left[\left[K_{n+1}\right]\left[K_n\right] \cdots \left[K_{a+2}\right]\left[K_{a+1}\right]\right]\left\{\alpha_a\left\{X_a\right\}_A + \frac{1}{R}\left\{X_a\right\}_B + V_a\left\{X_a\right\}_C + M_a\left\{X_a\right\}_D\right\} \tag{A8}$$

Thus, it is evident from equation (A8) that the solution at any established station along the length of the beam can always be written in terms of the sum of the appropriate lower boundary conditions.

REFERENCES

1. Arbic, Richard G.; White, George; and Gillespie, Warren, Jr.: Some Approximate Methods for Estimating the Effects of Aeroelastic Bending of Rocket-Propelled Model-Booster Combinations. NACA RM L53A08, 1953.

2. Thomson, K. D.: The Aero-Elastic Divergence of Slender Multi-Stage Test Vehicles. Tech. Note HSA-93, Weapons Res. Estab., Australian Defense Sci. Serv., Nov. 1962.

3. Alley, Vernon L., Jr.; and Gerringer, A. Harper: An Analysis of Aeroelastic Divergence in Unguided Launch Vehicles. NASA TN D-3281, 1966.

4. Keith, J. S.; et al.: Methods in Structural Dynamics for Thin Shell Clustered Launch Vehicles. FDL-TDR-64-105, U.S. Air Force, Apr. 1965.

5. Mechtly, E. A.: The International System of Units – Physical Constants and Conversion Factors. NASA SP-7012, 1964.

6. Muraca, Ralph J.: Aerodynamic Load Distributions for the Project FIRE Configurations at Mach Numbers From 0.25 to 4.63. NASA TN D-2604, 1965.

7. Alley, Vernon L., Jr.; Guillotte, Robert J.; and Hunter, Lessie D.: A Method of Determining Modal Data of a Nonuniform Beam With Effects of Shear Deformation and Rotary Inertia. NASA TN D-2930, 1965.

8. Leadbetter, Sumner A.; Alley, Vernon L., Jr.; Herr, Robert W.; and Gerringer, A. Harper: An Experimental and Analytical Investigation of the Natural Frequencies and Mode Shapes of a Four-Stage Solid-Propellant Rocket Vehicle. NASA TN D-1354, 1962.

9. Pitts, William C.; Nielsen, Jack N.; and Kaattari, George E.: Lift and Center of Pressure of Wing-Body-Tail Combinations at Subsonic, Transonic, and Supersonic Speeds. NACA Rept. 1307, 1957.

10. Falanga, Ralph A.; Hinson, William F.; and Crawford, Davis H.: Exploratory Tests of the Effects of Jet Plumes on the Flow Over Cone-Cylinder-Flare Bodies. NASA TN D-1000, 1962.

11. Hinson, William F.; and Hoffman, Sherwood: Analysis of Jet-Pluming Interference by Computer Simulation of Measured Flight Motions of Two RAM A Fourth Stages. NASA TN D-2018, 1963.

12. Muraca, Ralph J.: An Empirical Method for Determining Static Distributed Aerodynamic Loads on Axisymmetric Multistage Launch Vehicles. NASA TN D-3283, 1966.

13. Van Dyke, Milton D.: First- and Second-Order Theory of Supersonic Flow Past Bodies of Revolution. Aeron. Sci., vol. 18, no. 3, Mar. 1951, pp. 161-178, 216.

14. Savin, Raymond C.: Application of the Generalized Shock-Expansion Method to Inclined Bodies of Revolution Traveling at High Supersonic Airspeeds. NACA TN 3349, 1955.

15. Sauer, Robert: Introduction to Theoretical Gas Dynamics. J. W. Edwards (Ann Arbor, Mich.), 1947.

NASA-Langley, 1967 —— 32 L-4710

"The aeronautical and space activities of the United States shall be conducted so as to contribute . . . to the expansion of human knowledge of phenomena in the atmosphere and space. The Administration shall provide for the widest practicable and appropriate dissemination of information concerning its activities and the results thereof."

—NATIONAL AERONAUTICS AND SPACE ACT OF 1958

NASA SCIENTIFIC AND TECHNICAL PUBLICATIONS

TECHNICAL REPORTS: Scientific and technical information considered important, complete, and a lasting contribution to existing knowledge.

TECHNICAL NOTES: Information less broad in scope but nevertheless of importance as a contribution to existing knowledge.

TECHNICAL MEMORANDUMS: Information receiving limited distribution because of preliminary data, security classification, or other reasons.

CONTRACTOR REPORTS: Scientific and technical information generated under a NASA contract or grant and considered an important contribution to existing knowledge.

TECHNICAL TRANSLATIONS: Information published in a foreign language considered to merit NASA distribution in English.

SPECIAL PUBLICATIONS: Information derived from or of value to NASA activities. Publications include conference proceedings, monographs, data compilations, handbooks, sourcebooks, and special bibliographies.

TECHNOLOGY UTILIZATION PUBLICATIONS: Information on technology used by NASA that may be of particular interest in commercial and other non-aerospace applications. Publications include Tech Briefs, Technology Utilization Reports and Notes, and Technology Surveys.

Details on the availability of these publications may be obtained from:

SCIENTIFIC AND TECHNICAL INFORMATION DIVISION

NATIONAL AERONAUTICS AND SPACE ADMINISTRATION

Washington, D.C. 20546